Supplementary Information

Quenching of *syn*-Bimane Fluorescence by Na^+ Complexation

Ankana Roy,[a] Partha Jyoti Das,[a] Yael Diskin-Posner,[b] Michael Firer,[c] Flavio Grynszpan,[a,*] Michael Montag,[a,*]

[a] A. Roy, P. J. Das, Dr. F. Grynszpan, Dr. M. Montag
Department of Chemical Sciences
Ariel University
Ariel 40700, Israel
Fax: (+972)3-906-6634
E-mail: michaelmo@ariel.ac.il, flaviog@ariel.ac.il

[b] Dr. Y. Diskin-Posner
Department of Chemical Research Support
Weizmann Institute of Science
Rehovot 76100, Israel

[c] Prof. M. Firer
Department of Chemical Engineering and Biotechnology
Ariel University
Ariel 40700, Israel

Table of Contents

General procedures. Commercially available reagents were reagent grade or better, and were used without further purification. All organic solvents were HPLC grade, and were dried over molecular sieves (3Å or 4Å) prior to their use in fluorescence experiments. NMR solvents were also dried over molecular sieves. Water was deionized with a Treion TSDI column (Treitel Chemical Engineering; $\rho \geq 50$ kΩ cm). NMR spectra were processed with TopSpin 3.5 (Bruker Corp.), and plotted with MNova 11.0.4 (Mestrelab Research). Crystal structures were drawn and analyzed using Mercury CSD 3.9,[1] and Platon v. 91117.[2]

Analysis. NMR spectra (^{1}H, ^{13}C) were recorded using a Bruker Avance-III 400 MHz spectrometer, equipped with a 5 mm BBFO SmartProbe. All measurements were done at room temperature. ^{1}H and ^{13}C NMR chemical shifts are reported in ppm relative to tetramethylsilane. ^{1}H NMR chemical shifts are referenced to the residual hydrogen signal of the deuterated solvent, and the ^{13}C NMR chemical shifts are referenced to the ^{13}C signal(s) of the deuterated solvent. Abbreviations used in the description of NMR data are as follows: Ar, aryl; s, singlet; d, doublet; t, triplet; q, quartet; m, multiplet.

UV-Vis absorbance spectra were measured with a Varian Cary 100 Bio UV-Visible Spectrophotometer, at a scan rate of 600 nm/min. 1- and 10-mm-pathlength quartz cuvettes were used for 1 mM and 5 μM *syn*-(Me,Me)bimane solutions, respectively.

Infrared spectra were recorded in the attenuated total reflectance (ATR) mode using a Bruker Vertex 70 FT-IR spectrometer, fitted with a PLATINUM Diamond ATR accessory, at a resolution of 4 cm^{-1}.

Differential scanning calorimetry (DSC) measurements were carried out using a Mettler Toledo TGA/DSC 1 STAR system, employing a heating rate of 10 °/min, under a flow of dry N_2 (10 ml/min).

Elemental analyses were performed using a ThermoFischer Scientific FlashSmart CHNS Elemental Analyzer. Some analyses were also performed at the Interdepartmental Equipment Facility, Faculty of Agriculture, Food and Environment, The Hebrew University of Jerusalem, as well as at the Scientific Equipment Center, Department of Chemistry, Bar-Ilan University.

Powder X-ray diffraction measurements were conducted at the Department of Chemical Research Support, Weizmann Institute of Science. Diffraction data were

[1] C. F. Macrae, I. J. Bruno, J. A. Chisholm, P. R. Edgington, P. McCabe, E. Pidcock, L. Rodriguez-Monge, R. Taylor, J. van de Streek and P. A. Wood, *J. Appl. Cryst.*, 2008, **41**, 466-470.

[2] (a) A. L. Spek, *J. Appl. Cryst.* 2003, **36**, 7-13. (b) A. L. Spek, *Acta Cryst.* 2009, **D65**, 148-155.

collected at room temperature using a Rigaku ULTIMA III (2kW) theta-theta vertical diffractometer with a sealed Cu-anode tube (line source).
Crystal structures from the Cambridge Structural Database (CSD; v. 5.38, May 2017),[3] were retrieved by using ConQuest v. 1.19.[4]

Fluorescence measurements. Fluorescence spectra were recorded on a Varian Cary Eclipse Fluorescence Spectrophotometer, using a 2.5-nm excitation slit width, a 5-nm emission slit width, and a 120 nm/min scan rate.
For experiments involving 1 mM solutions of *syn*-(Me,Me)bimane, samples were placed in a 0.1-mm-pathlength absorbance quartz cuvette, which was tilted at 60° relative to the incident excitation beam (front-face illumination),[5] by using a specially-built cuvette holder. This setup was designed to keep the total absorbance at the excitation wavelengths below 0.1, so as to minimize inner filter effects in the relatively concentrated 1 mM solutions, while also minimizing interference from the scattered excitation light. The same setup was used for solid samples, after suspending them in mineral oil prior to measurement.
For experiments involving 5 μM solutions of *syn*-(Me,Me)bimane, a standard 10-mm fluorescence cuvette was used, employing a normal 90° illumination mode.
The observed changes in bimane emission intensity upon addition of $NaBPh_4$ were also accompanied by changes in bimane absorbance. All fluorescence spectra were corrected for these absorbance variations by dividing the experimental emission intensity by $1 - 10^{-A_{ex}}$, where A_{ex} is the absorbance of *syn*-(Me,Me)bimane at the excitation wavelength.[6] When 1 mM bimane solutions were employed, the added $NaBPh_4$ did not contribute significantly to the overall absorbance at the excitation wavelength. However, when the concentration of bimane was lowered to 5 μM, the relative absorbance of $NaBPh_4$ at the excitation wavelength could no longer be neglected. Therefore, A_{ex} was calculated by subtracting the corresponding absorbance of $NaBPh_4$ from the total absorbance of the bimane/$NaBPh_4$ mixture.

Quantitative NMR measurements. Each of the sodium-bimane complexes was subjected to quantitative ^{1}H NMR spectroscopy, in order to assess the composition

[3] F. H. Allen, *Acta Crystallogr., Sect. B: Struct. Sci.*, 2002, **58**, 380-388.
[4] I. J. Bruno, J. C. Cole, P. R. Edgington, M. Kessler, C. F. Macrae, P. McCabe, J. Pearson and R. Taylor, *Acta Crystallogr., Sect. B: Struct. Sci.*, 2002, **58**, 389-397.
[5] J. R. Lakowicz, *Principles of Fluorescence Spectroscopy*, Springer, New York, 3rd edn., 2006, Ch. 2, pp. 27-61.
[6] S. W. Bigger, K. P. Ghiggino, G. A. Meilak and B. Verity, *J. Chem. Educ.*, 1992, **69**, 675-677.

and purity of bulk samples of these complexes. Each sample typically comprised 2-5 mg of crystals, dissolved in CD_3CN. Dimethyl sulfone (SO_2Me_2) was employed as the integration standard, and the measurements were carried out using a long 30-sec delay time between consecutive scans.

Solvent for routine NMR measurements. In order to observe the effects of bimane coordination to Na^+, a relatively nonpolar NMR solvent was required, such as $CDCl_3$. To ensure acceptable signal-to-noise ratios during routine NMR measurements, bimane concentration was set at 8 mM. In $CDCl_3$, this often resulted in spontaneous crystallization of the sodium-bimane complexes during measurement. To prevent this, without substantially affecting solvent polarity, we used a mixture of 20% (v/v) 1,2-dichloroethane ($C_2H_4Cl_2$) in $CDCl_3$.

Synthesis of *syn*-(Me,Me)bimane (1). *syn*-(Me,Me)bimane was synthesized using a literature procedure.[7] Room-temperature NMR data are given below for this compound in 20% $C_2H_4Cl_2/CDCl_3$. The ^1H and ^{13}C NMR signals are assigned to atomic positions in the bimane scaffold that are enumerated relative to the carbonyl groups, as represented in Figure S1.

^1H NMR (400 MHz, 20% $C_2H_4Cl_2/CDCl_3$, 8 mM): 2.26 (m, 6H, CH_3, γ), 1.80 (m, 6H, CH_3, β'). $^{13}C\{^1H\}$ NMR (101 MHz, 20% $C_2H_4Cl_2/CDCl_3$, 8 mM): 160.86 (s, *C*=O), 145.92 (s, *C*=C, β), 112.64 (s, *C*=C, α), 11.86 (s, *C*H_3, γ), 6.77 (s, *C*H_3, β'). The $^{13}C\{^1H\}$ NMR data were obtained from a DEPTQ experiment. Assignment of the ^1H and $^{13}C\{^1H\}$ NMR signals was confirmed by an HMBC experiment. See Figures S2 and S3 for the experimental NMR spectra.

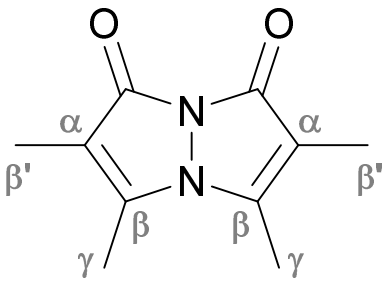

Figure S1. Structure of *syn*-(Me,Me)bimane, showing the enumeration of atomic positions relative to the carbonyl groups.

[7] E. M. Kosower and B. Pazhenchevsky, *J. Am. Chem. Soc.*, 1980, **102**, 4983-4993.

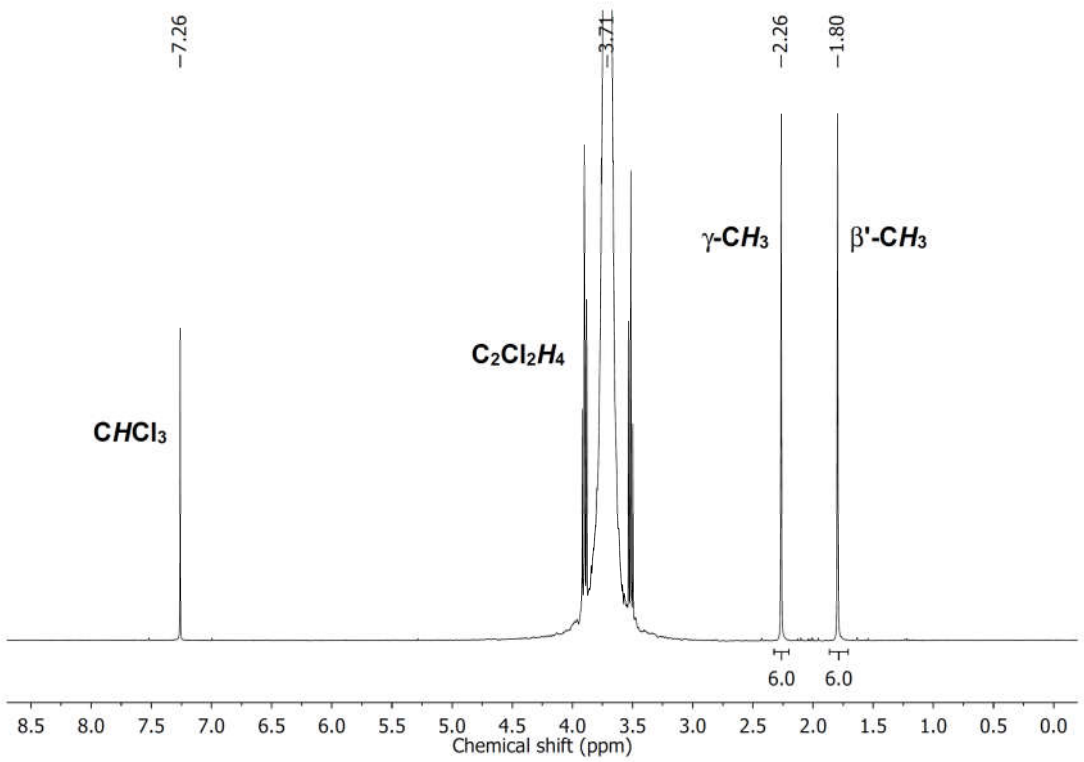

Figure S2. ^{1}H NMR spectrum of 8 mM *syn*-(Me,Me)bimane in 20% $C_2H_4Cl_2/CDCl_3$.

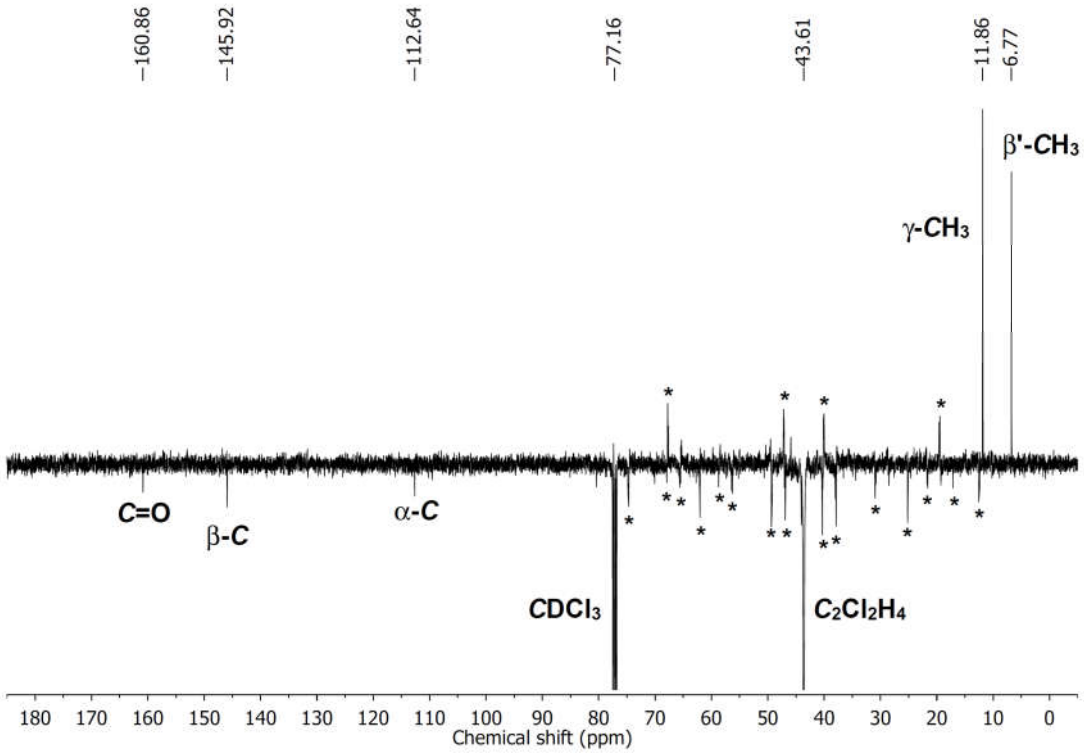

Figure S3. $^{13}C\{^{1}H\}$ DEPTQ NMR spectrum of 8 mM *syn*-(Me,Me)bimane in 20% $C_2H_4Cl_2/CDCl_3$. Signals marked with asterisks (*) are artifacts caused by the intense peak of $C_2H_4Cl_2$.

Synthesis of complex 2, $[Na_2(bimane)_6](BPh_4)_2$. 280 mg (1.46 mmol) of *syn*-(Me,Me)bimane were dissolved in 70 ml of dry THF, and then 166 mg (0.485 mmol) of solid $NaBPh_4$ were added to the solution, with stirring. The resulting solution, which immediately changed from colorless to yellow, was stirred at room temperature for 10 min. The solvent was then evaporated under reduced pressure, until the solution reached about a third of its original volume. The product was crystallized at room temperature by allowing diethyl ether vapors to slowly diffuse into the concentrated THF solution, affording yellow feather-like crystals within a few days. The crystals were then separated from the mother-liqueur, washed three times with hexane/$CHCl_3$ (40:60, v/v), twice with diethyl ether, and placed under vacuum to remove residual solvent. This gave 415 mg (0.215 mmol; 89% yield)[8] of the product, complex **2**.

The ^1H and ^{13}C NMR signals are assigned to atomic positions in the bimane scaffold that are enumerated relative to the carbonyl groups (Figure S1).

^1H NMR (400 MHz, 20% $C_2H_4Cl_2/CDCl_3$, 1.3 mM): 7.33 (m, 16H, $B(C_6H_5)_4^-$, *ortho*), 6.92 (t, $^3J_{HH}$ = 7.4 Hz, 16H, $B(C_6H_5)_4^-$, *meta*), 6.76 (m, $^3J_{HH}$ = 7.2 Hz, 8H, $B(C_6H_5)_4^-$, *para*), 2.11 (m, 36H, CH_3, γ), 1.75 (m, 36H, CH_3, β'). $^{13}C\{^1H\}$ NMR (101 MHz, 20% $C_2H_4Cl_2/CDCl_3$, 1.3 mM): 164.17 (m, B–C_{Ar}), 162.12 (s, *C*=O), 147.87 (s, *C*=C, β), 135.98 (s, C_{Ar}–H, *ortho*), 125.53 (m, C_{Ar}–H, *meta*), 121.65 (s, C_{Ar}–H, *para*), 112.38 (s, *C*=C, α), 11.79 (s, CH_3, γ), 6.54 (s, CH_3, β'). The $^{13}C\{^1H\}$ NMR data were obtained from a DEPTQ experiment. Assignment of the ^1H and $^{13}C\{^1H\}$ NMR signals was confirmed by an HMBC experiment. See Figures S4 and S5 for the experimental NMR spectra.

Anal. calcd for $C_{108}H_{112}B_2N_{12}Na_2O_{12}$: C, 70.59%; H, 6.14%; N, 9.15%. Found: C, 70.75%; H, 6.24%; N, 9.24%.

Melting point: 186 °C

[8] Based on qNMR data, the purity of the product was 95%. The molar and percent yields were calculated assuming this level of purity.

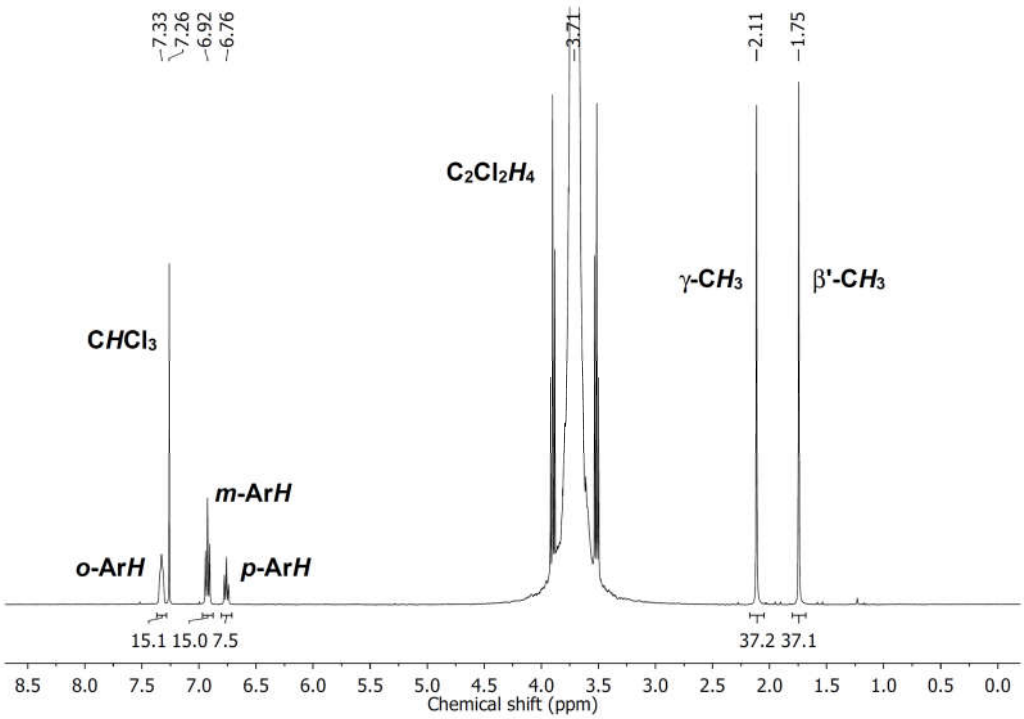

Figure S4. ^{1}H NMR spectrum of 1.3 mM complex **2** in 20% $C_2H_4Cl_2/CDCl_3$.

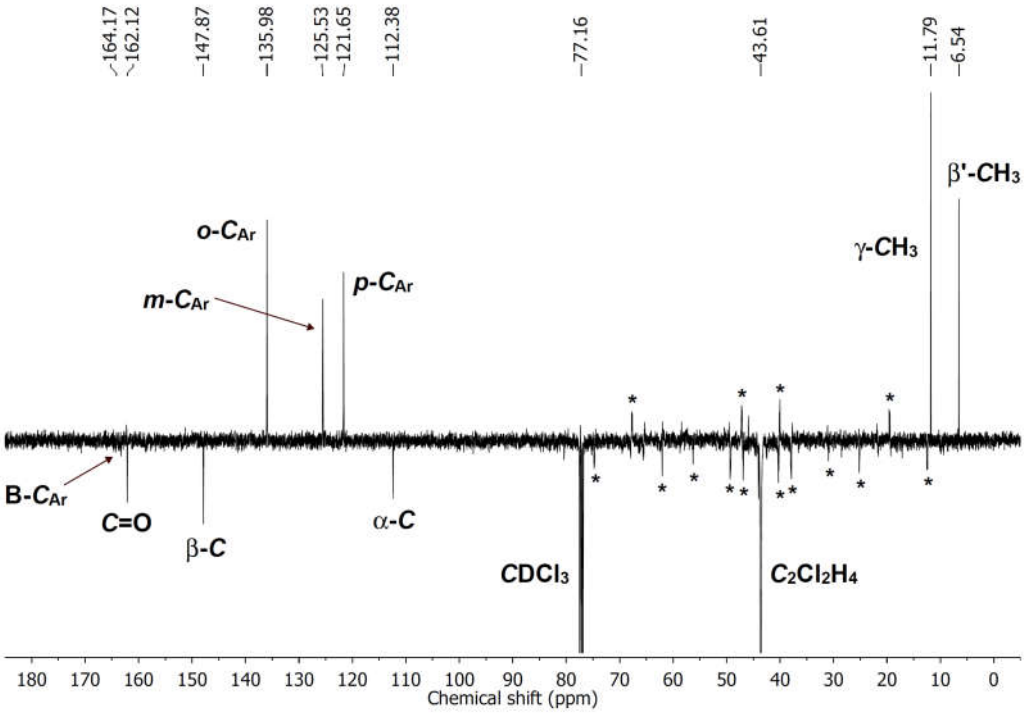

Figure S5. $^{13}C\{^{1}H\}$ DEPTQ NMR spectrum of 1.3 mM complex **2** in 20% $C_2H_4Cl_2/CDCl_3$. The resonance for B–C_{Ar} at 164.17 ppm was located and assigned on the basis of a ^{13}C-^{1}H HMBC experiment. Signals marked with asterisks (*) are artifacts caused by the intense peak of $C_2H_4Cl_2$.

Synthesis of complex 3, $[Na_2(bimane)_4(CH_3CN)_2](BPh_4)_2 \bullet xCH_3CN$. 70.9 mg (0.369 mmol) of *syn*-(Me,Me)bimane were dissolved in 12 ml of dry acetonitrile, and then 63.1 mg (0.184 mmol) of solid $NaBPh_4$ were added to the solution, with stirring. The resulting solution, which immediately changed from colorless to light yellow, was stirred at room temperature for 10 min. The solvent was then evaporated under reduced pressure, until the solution reached about a third of its original volume. The product was crystallized at room temperature by allowing diethyl ether vapors to slowly diffuse into the concentrated acetonitrile solution, affording yellowish-green needle-like crystals within a few days. The crystals were then separated from the mother-liqueur, washed once with hexane/$CHCl_3$ (40:60, v/v), twice with diethyl ether, and air-dried. This gave 136 mg (0.0833 mmol; 90% yield)[9] of the product, complex **3**.

The ^1H and ^{13}C NMR signals are assigned to atomic positions in the bimane scaffold that are enumerated relative to the carbonyl groups (Figure S1).

^1H NMR (400 MHz, 20% $C_2H_4Cl_2/CDCl_3$, 2 mM): 7.36 (m, 16H, $B(C_6H_5)_4^-$, *ortho*), 6.94 (t, $^3J_{HH}$ = 7.4 Hz, 16H, $B(C_6H_5)_4^-$, *meta*), 6.76 (m, $^3J_{HH}$ = 7.2 Hz, 8H, $B(C_6H_5)_4^-$, *para*), 2.03 (m, 24H, CH_3, γ), 1.96 (s, 9H, CH_3CN),[10] 1.71 (m, 24H, CH_3, β').

$^{13}C\{^1H\}$ NMR (101 MHz, 20% $C_2H_4Cl_2/CDCl_3$, 2 mM): 164.02 (q, $^1J_{BC}$ = 49.2 Hz, B–C_{Ar}), 162.76 (s, *C*=O), 148.98 (s, *C*=C, β), 135.85 (s, C_{Ar}–H, *ortho*), 125.72 (m, C_{Ar}–H, *meta*), 121.75 (s, C_{Ar}–H, *para*), 116.39 (s, CH_3CN), 112.23 (s, *C*=C, α), 11.76 (s, CH_3, γ), 6.41 (s, CH_3, β'), 1.85 (s, CH_3CN). The $^{13}C\{^1H\}$ NMR data were obtained from a DEPTQ experiment. Assignment of the ^1H and $^{13}C\{^1H\}$ NMR signals was confirmed by an HMBC experiment. See Figures S6 and S7 for the experimental NMR spectra.

Satisfactory elemental analyses could not be obtained for this complex, due to facile loss of the co-crystallized acetonitrile.

Melting point: 218 °C (decomp)

---

[9] Due to facile loss of the co-crystallized interstitial acetonitrile, bulk samples of complex **3** differed in their CH_3CN content. qNMR data for these samples showed the bimane-to-CH_3CN molar ratio to typically vary between 1:1 and 2:1, whereas the bimane-to-BPh_4^- molar ratio was consistently 2:1, as expected. The molar and percent yields reported here were calculated assuming a purity of 94%, as estimated by qNMR. The calculation was based on the detected amounts of bimane and BPh_4^-, and a molecular composition excluding interstitial CH_3CN, i.e., $[Na_2(bimane)_4(CH_3CN)_2](BPh_4)_2$.

[10] On the basis of the crystallographic data for complex **3**, the bimane and CH_3CN are expected to be in equimolar amounts. Therefore, the ratio of integrals for their respective ^1H NMR signals should be 4:1 (12H per bimane molecule, 3H per acetonitrile molecule). However, the observed amount of CH_3CN is ~25% lower than expected due to facile loss of this volatile component.

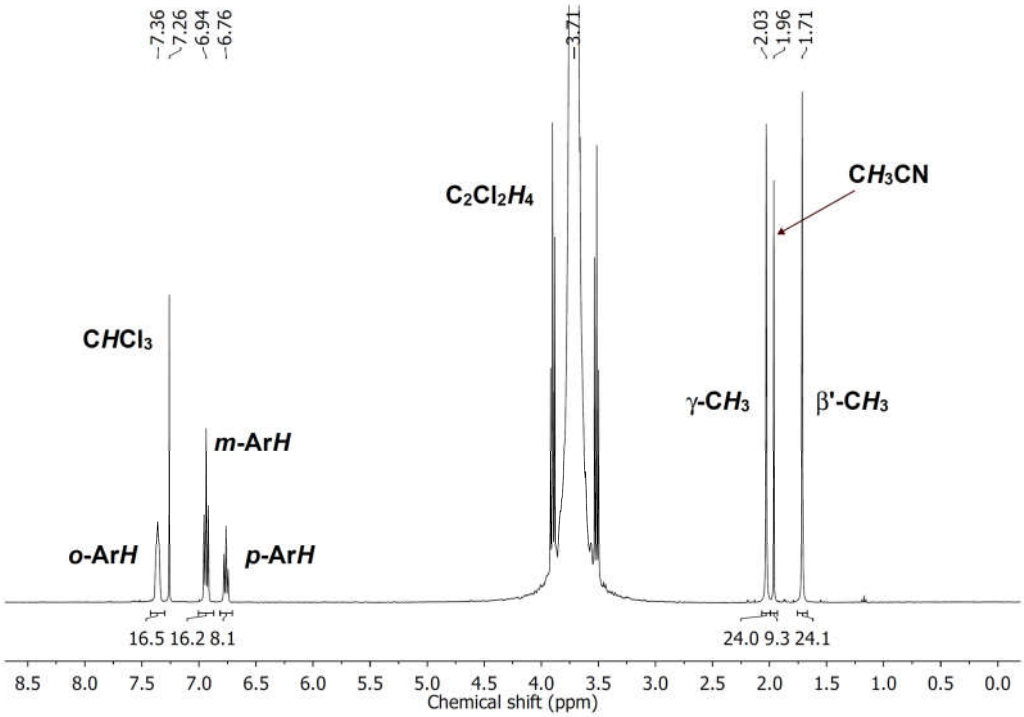

Figure S6. ^{1}H NMR spectrum of 2 mM complex **3** in 20% $C_2H_4Cl_2/CDCl_3$. Note that the integral for the CH_3CN peak is therefore 9.3, instead of the expected 12.0, reflecting the tendency of this complex to lose acetonitrile in the solid state.

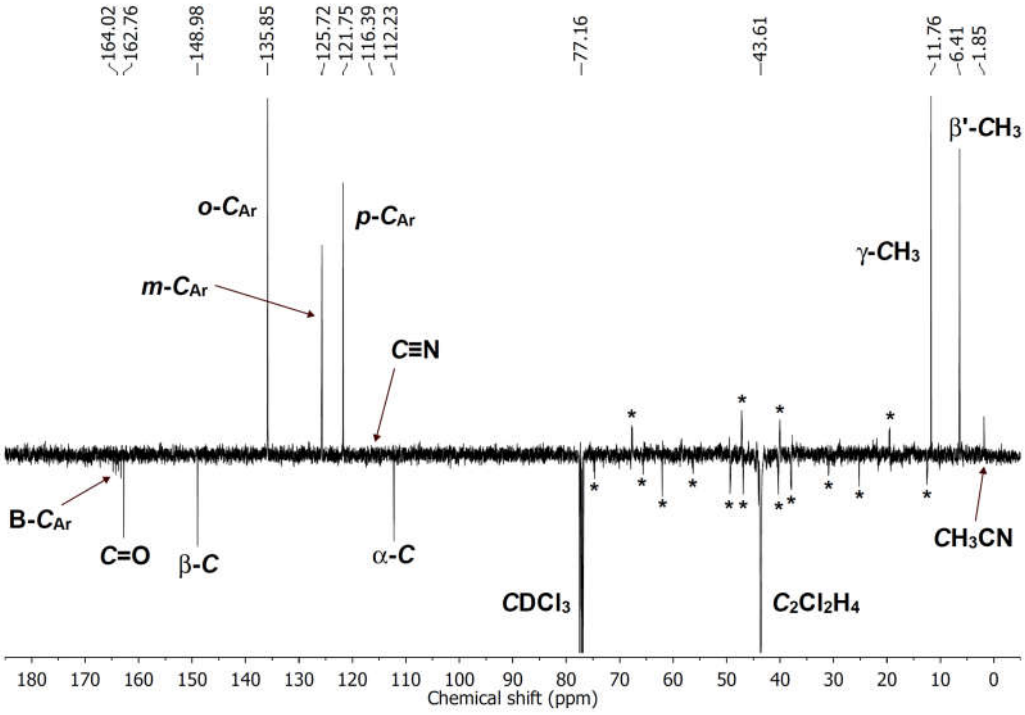

Figure S7. $^{13}C\{^{1}H\}$ DEPTQ NMR spectrum of 2 mM complex **3** in 20% $C_2H_4Cl_2/CDCl_3$. The C≡N resonance at 116.39 ppm was located and assigned on the basis of a ^{13}C-^{1}H HMBC experiment. Signals marked with asterisks (*) are artifacts caused by the intense peak of $C_2H_4Cl_2$.

Synthesis of complex 4, [Na(bimane)$_2$]BPh$_4$. 300 mg (0.185 mmol) of complex **3** were dissolved in 120 ml of dry chloroform. The product was crystallized at room temperature by allowing diethyl ether vapors to slowly diffuse into the chloroform solution, affording greenish-yellow block-shaped crystals within a few days. The crystals were then separated from the mother-liqueur, washed three times with $CHCl_3$, twice with diethyl ether, and placed under vacuum to remove residual solvent. This gave 144 mg (0.192 mmol; 52% yield)[11] of the product, complex **4**.

The ^{1}H and ^{13}C NMR signals are assigned to atomic positions in the bimane scaffold that are enumerated relative to the carbonyl groups (Figure S1).

^{1}H NMR (400 MHz, 20% $C_2H_4Cl_2$/$CDCl_3$, 4 mM): 7.40 (m, 8H, $B(C_6H_5)_4^-$, *ortho*), 6.96 (t, $^3J_{HH}$ = 7.4 Hz, 8H, $B(C_6H_5)_4^-$, *meta*), 6.78 (m, $^3J_{HH}$ = 7.2 Hz, 4H, $B(C_6H_5)_4^-$, *para*), 2.08 (m, 12H, CH_3, γ), 1.73 (m, 12H, CH_3, β'). ^{13}C{^{1}H} NMR (101 MHz, 20% $C_2H_4Cl_2$/$CDCl_3$, 4 mM): 163.82 (m, B–C_{Ar}), 162.61 (s, *C*=O), 148.72 (s, *C*=C, β), 135.76 (s, C_{Ar}–H, *ortho*), 125.83 (m, C_{Ar}–H, *meta*), 121.83 (s, C_{Ar}–H, *para*), 112.33 (s, *C*=C, α), 11.79 (s, *C*H$_3$, γ), 6.44 (s, *C*H$_3$, β'). The ^{13}C{^{1}H} NMR data were obtained from a DEPTQ experiment. Assignment of the ^{1}H and ^{13}C{^{1}H} NMR signals was confirmed by an HMBC experiment. See Figures S8 and S9 for the experimental NMR spectra.

Anal. calcd for $C_{44}H_{44}BN_4NaO_4$: C, 72.73%; H, 6.10%; N, 7.71%. Found: C, 71.82%; H, 6.01%; N, 7.57%.

Melting point: 215 °C

[11] Based on qNMR data, the purity of the product was 97%. The molar and percent yields were calculated assuming this level of purity.

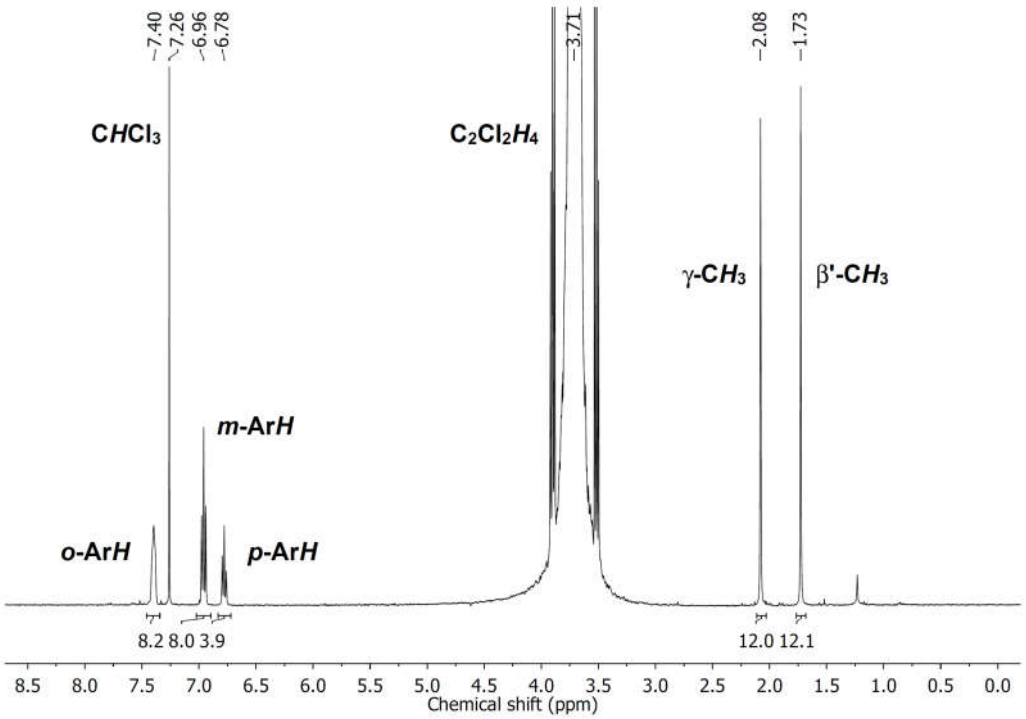

Figure S8. ^{1}H NMR spectrum of 4 mM complex **4** in 20% $C_2H_4Cl_2$/$CDCl_3$.

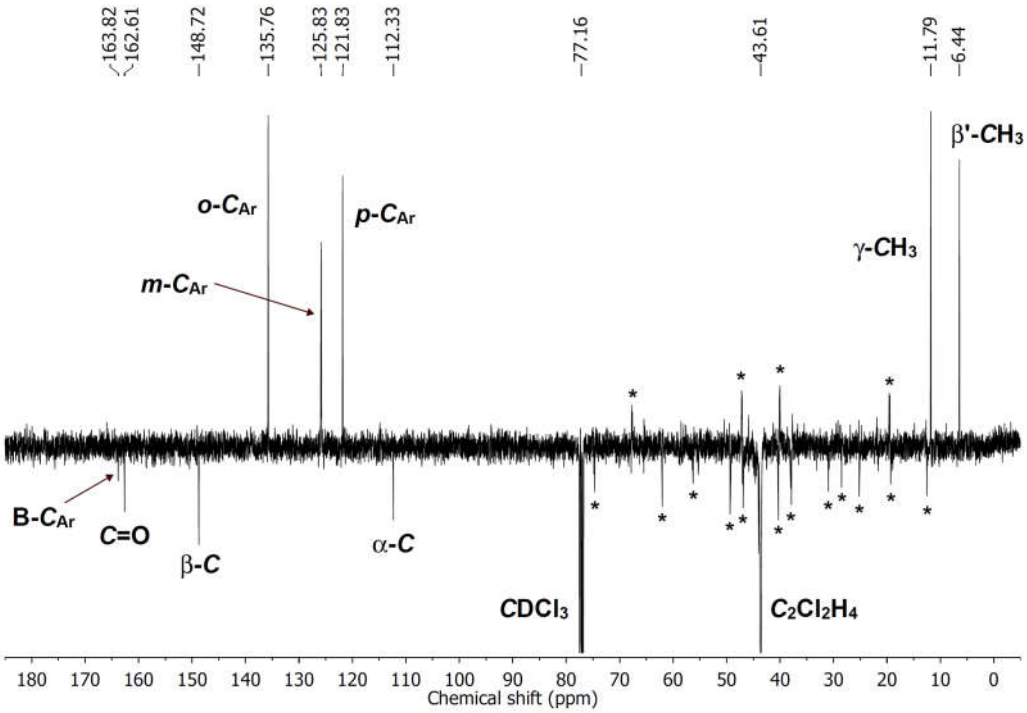

Figure S9. $^{13}C\{^{1}H\}$ DEPTQ NMR spectrum of 4 mM complex **4** in 20% $C_2H_4Cl_2$/$CDCl_3$. Signals marked with asterisks (*) are artifacts caused by the intense peak of $C_2H_4Cl_2$.

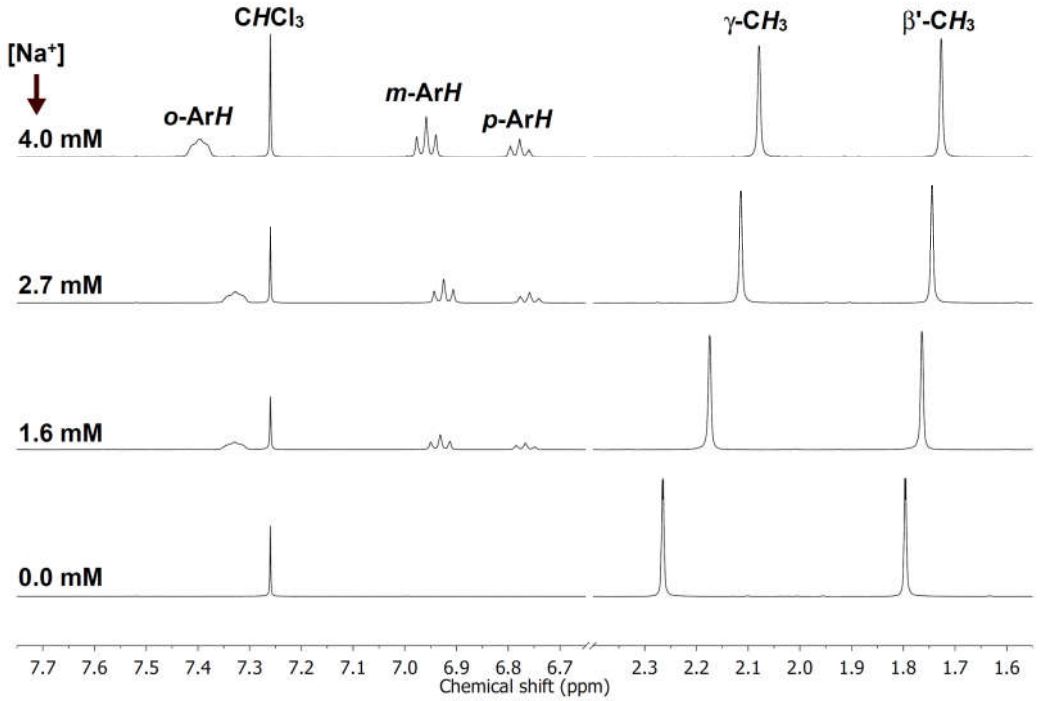

Figure S10. ^{1}H NMR spectra of 8 mM *syn*-(Me,Me)bimane in 20% $C_2H_4Cl_2/CDCl_3$, with increasing concentrations of $NaBPh_4$. The spectral region of 2.4-6.7 ppm, containing the strong dichloroethane resonance, was truncated for clarity.

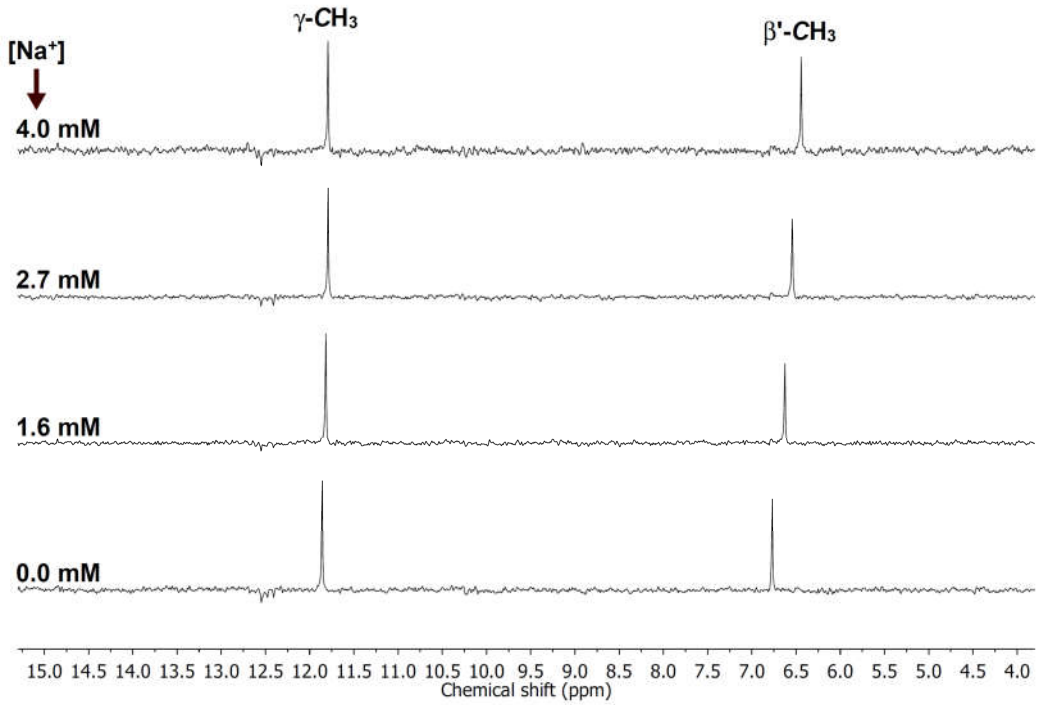

Figure S11. $^{13}C\{^{1}H\}$ DEPTQ NMR spectra of 8 mM *syn*-(Me,Me)bimane in 20% $C_2H_4Cl_2/CDCl_3$, with increasing concentrations of $NaBPh_4$. Only the highfield region containing the bimane methyl resonances is shown (see Figure S12 for the lowfield region).

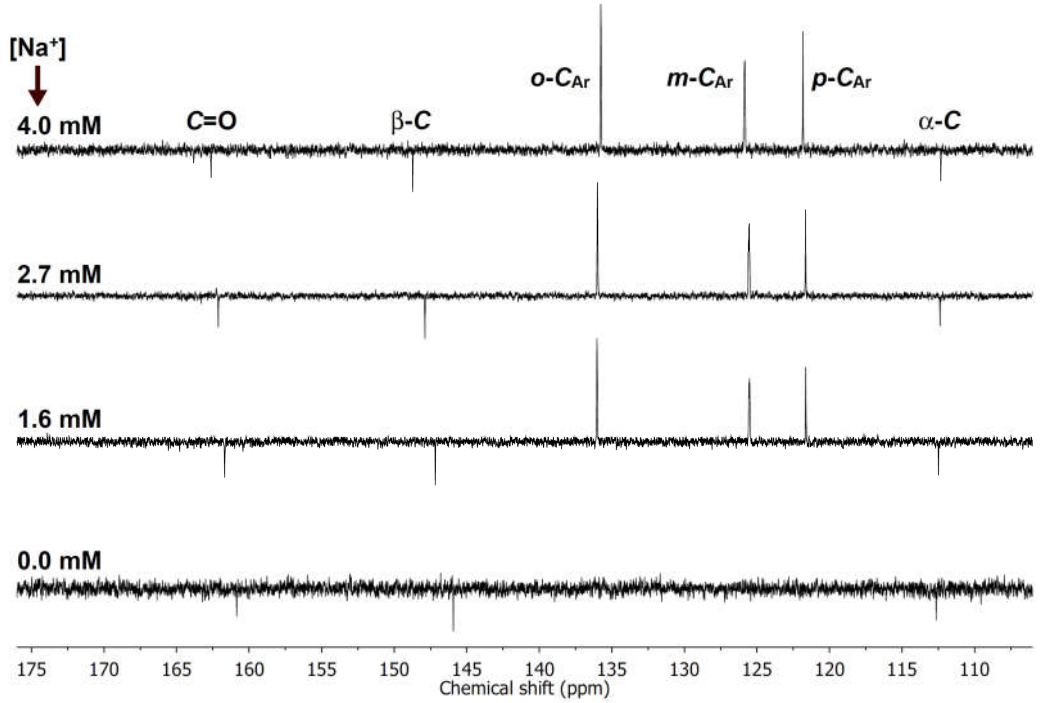

Figure S12. $^{13}C\{^{1}H\}$ DEPTQ NMR spectra of 8 mM *syn*-(Me,Me)bimane in 20% $C_2H_4Cl_2/CDCl_3$, with increasing concentrations of $NaBPh_4$. Only the lowfield region containing the bimane carbonyl and olefinic resonances, as well as the tetraphenylborate aromatic signals, is shown (see Figure S11 for the highfield region).

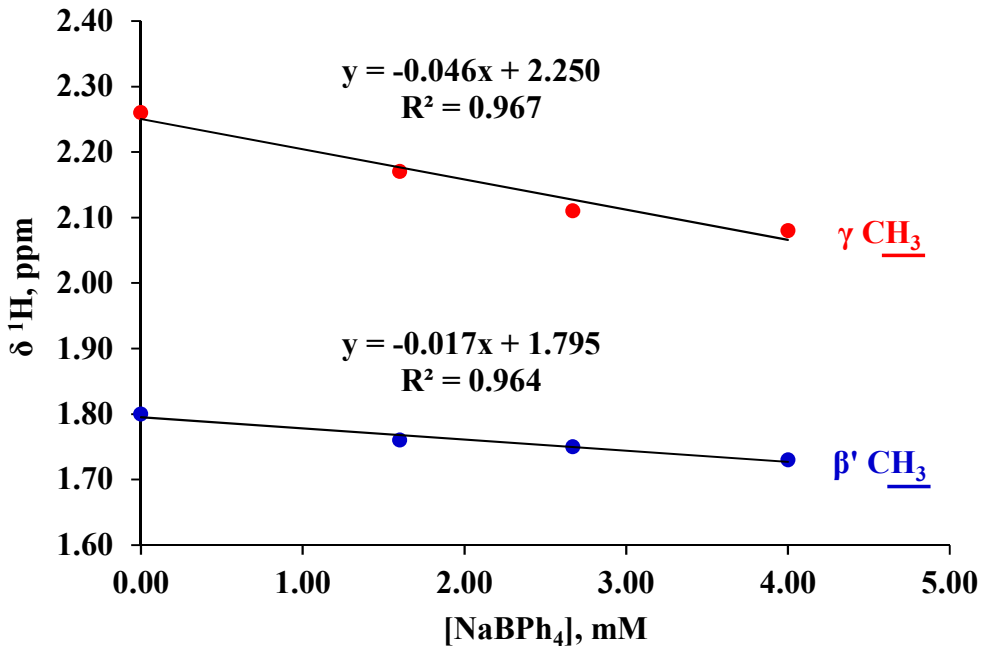

Figure S13. ^{1}H NMR chemical shifts of 8 mM *syn*-(Me,Me)bimane in 20% $C_2H_4Cl_2/CDCl_3$ as a function of $NaBPh_4$ concentration.

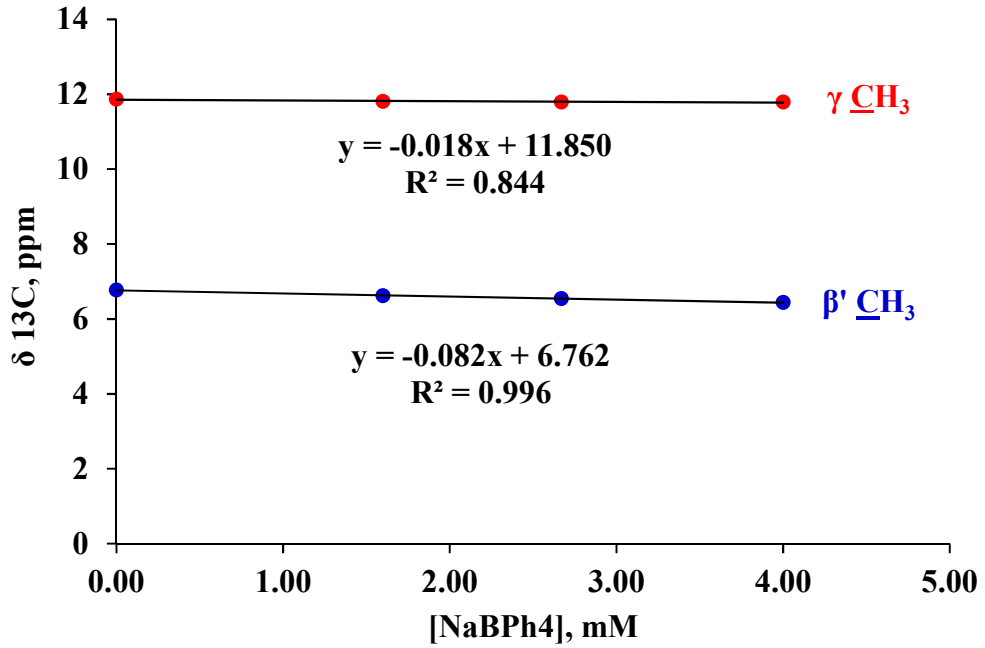

Figure S14. ^{13}C NMR chemical shifts of the methyl resonances of 8 mM *syn*-(Me,Me)bimane in 20% $C_2H_4Cl_2/CDCl_3$ as a function of $NaBPh_4$ concentration.

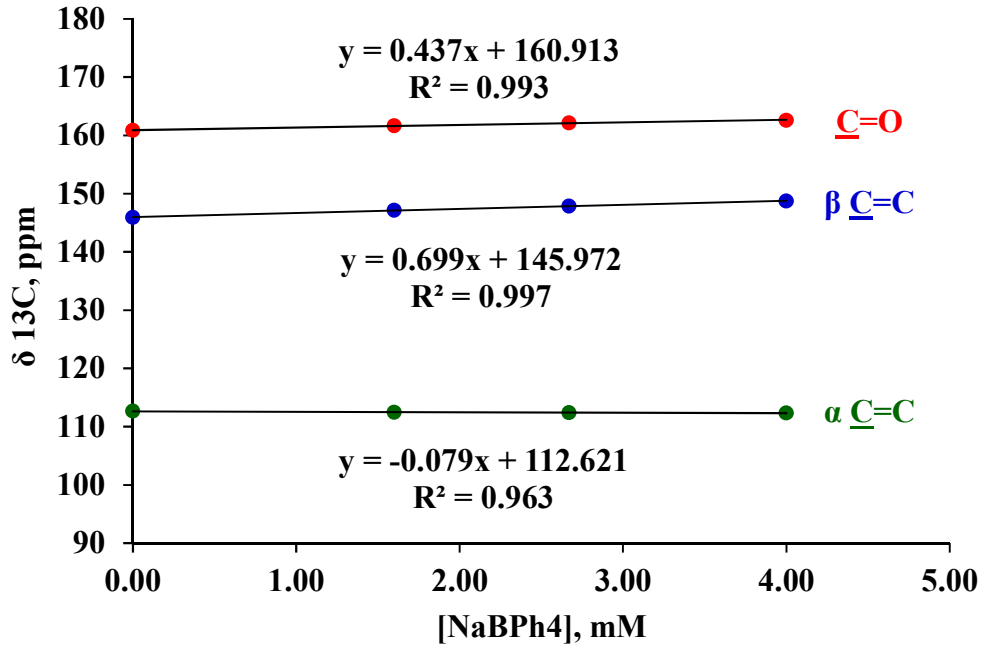

Figure S15. ^{13}C NMR chemical shifts of the endocyclic resonances of 8 mM *syn*-(Me,Me)bimane in 20% $C_2H_4Cl_2/CDCl_3$ as a function of $NaBPh_4$ concentration.

Crystal structure determination. Single-crystal X-ray diffraction experiments were carried out at the Department of Chemical Research Support, Weizmann Institute of Science. Crystallographic data were collected at 100 K on a dual source Rigaku XtaLab PRO diffractometer equipped with a PILATUS 200 detector, with radiation at

λ(Cu Kα) = 1.54184 Å. Data were processed with CrysAlis^{PRO}.[12] Structures were solved with SHELXT,[13] and refined using SHELXL,[14] with full matrix least-squares based on F^2. Hydrogen atoms were calculated in a riding mode. All crystallographic data were deposited in the CSD.

X-ray crystallographic analysis of *syn*-(Me,Me)bimane. The room-temperature crystal structure of *syn*-(Me,Me)bimane was reported previously.[15] Herein, we provide crystallographic data for this bimane at 100 K. Crystals of *syn*-(Me,Me)bimane suitable for X-ray diffraction were grown from an acetonitrile solution at -20 °C. The crystal parameters are given in Table S1, and the low-temperature crystal structure of the bimane is shown in Figure S16. The bimane scaffold bond lengths are collected in Table S2. For comparative purposes, this table also contains data for the previously-reported room-temperature structure.

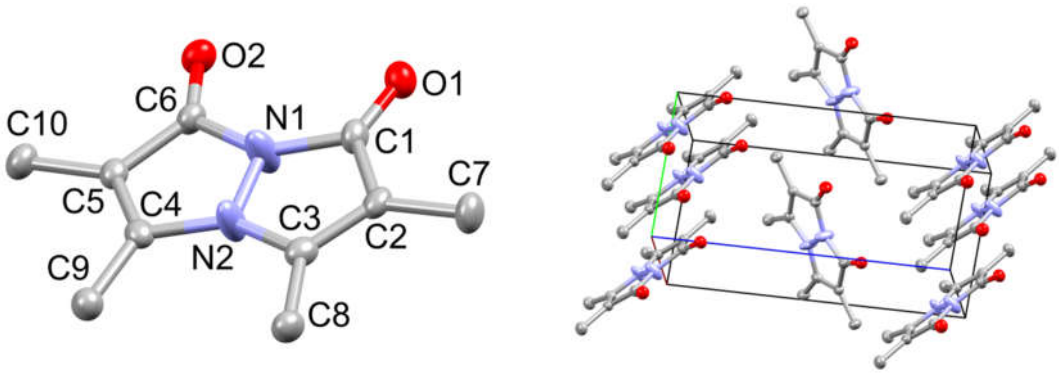

(a) (b)

Figure S16. Crystal structure of *syn*-(Me,Me)bimane at 100 K (with thermal ellipsoids at the 50% probability level): (a) asymmetric unit; (b) unit cell. Hydrogen atoms were omitted for clarity. Atoms are color-coded as follows: O, red; C, grey; N, light blue.

[12] CrysAlisPRO, Oxford Diffraction / Agilent Technologies UK Ltd, Yarnton, England.
[13] G. M. Sheldrick, *Acta Crystallogr., Sect. A: Fundam. Crystallogr.*, 2015, **71**, 3-8.
[14] G. M. Sheldrick, *Acta Crystallogr., Sect. C: Cryst. Struct. Commun.*, 2015, **71**, 3-8.
[15] J. Bernstein, E. Goldstein and I. Goldberg, *Cryst. Struct. Commun.*, 1980, **9**, 301-305.

Table S1. Crystallographic data for *syn*-(Me,Me)bimane (**1**) and complexes **2**-**4**.

	***syn*-(Me,Me)bimane (1)**	**Complex 2**	**Complex 3**	**Complex 4 (polymorph A)**	**Complex 4 (polymorph B)**
Formula	$C_{10}H_{12}N_2O_2$	$C_{108}H_{112}B_2N_{12}Na_2O_{12}$	$C_{96}H_{100}B_2N_{12}Na_2O_8$	$C_{44}H_{44}BN_4NaO_4$	$C_{44}H_{44}BN_4NaO_4$
FW, g mol^{-1}	192.22	1837.69	1617.47	726.63	726.63
Crystal appearance	Colorless plate	Light yellow plate	Yellow needle	Light green prism	Yellow block
Crystal dimensions, mm	0.099 × 0.072 × 0.052	0.323 × 0.055 × 0.023	0.162 × 0.027 × 0.027	0.199 × 0.077 × 0.069	0.125 × 0.066 × 0.038
Crystal system	Monoclinic	Monoclinic	Monoclinic	Monoclinic	Monoclinic
Space group	*Pn*	*P2$_1$/n*	*Pc*	*C2/c*	*C2/c*
a, Å	6.51250(10)	15.2728(2)	14.8036(3)	17.4802(1)	17.4616(3)
b, Å	5.97220(10)	10.3419(1)	10.3215(2)	11.8861(1)	11.9083(1)
c, Å	12.10290(10)	30.0963(3)	28.7105(6)	19.0909(2)	20.9140(3)
α, °	90.0	90.0	90.0	90.0	90.0
β, °	95.6560(10)	98.513(1)	91.843(2)	110.406(1)	121.268(2)
γ, °	90.0	90.0	90.0	90.0	90.0
Cell volume, Å^3	468.438(11)	4701.33(9)	4384.56(15)	3717.62(6)	3717.14(11)
Z	2	2	2	4	4
D (calc), g cm^{-3}	1.363	1.298	1.225	1.298	1.298
μ, mm^{-1}	0.794	0.760	0.710	0.761	0.761
Temperature, K	100(2)	100(2)	100(2)	100(2)	100(2)
Radiation	Cu Kα (λ = 1.54184 Å)	Cu Kα (λ = 1.54184 Å)	Cu Kα (λ = 1.54184 Å)	Cu Kα (λ = 1.54184 Å)	Cu Kα (λ = 1.54184 Å)
F(000)	204	1944	1712	1536	1536
Limiting indices	-8≤h≤8, -7≤k≤7, -15≤l≤15	-19≤h≤19, -12≤k≤12, -38≤l≤29	-17≤h≤17, -9≤k≤12, -34≤l≤34	-21≤h≤16, -14≤k≤12, -23≤l≤23	-19≤h≤21, -11≤k≤14, -26≤l≤14
Reflections (unique)	8323 (1801)	41296 (10062)	34188 (14697)	15105 (3532)	15961(3795)
Data completeness	0.999	0.998	0.997	1.000	1.000
θ_{max}, °	79.9	80.2	66.6	70.1	74.473
R_{int}	0.0267	0.0390	0.0471	0.0343	0.0272
Data/restraints/parameters	1801 / 2 / 131	10062 / 0 / 633	14697 / 2 / 1117	3532 / 0 / 249	3795 / 0 / 249
R_1,* wR_2** (all data)	0.0410, 0.1024	0.0525, 0.1201	0.0740, 0.1461	0.0387, 0.0993	0.0401, 0.0989
R_1,* wR_2** [$F^2 > 2\sigma(F^2)$]	0.0403, 0.1020	0.0451, 0.1158	0.0559, 0.1354	0.0370, 0.0981	0.0374, 0.0970
Goodness-of-fit on F^2***	1.090	1.048	1.025	1.042	1.049
Largest peak / hole, e Å^{-3}	0.230 / -0.176	0.358 / -0.286	0.329 / -0.194	0.240 / -0.345	0.275 / -0.374
Flack parameter	0.03(11)	-	0.5(2)	-	-
CCDC number	1821932	1821936	1821935	1821933	1821934

* $R_1 = \sum||F_0| - |F_c|| \,/\, \sum|F_0|$.

** $wR_2 = [\sum w({F_0}^2 - {F_c}^2)^2 \,/\, \sum w({F_0}^2)^2]^{1/2}$.

*** Goodness-of-fit = $S = [\sum w\left({F_0}^2 - {F_c}^2\right)^2 /(n-p)]^{1/2}$; n = number of reflections; p = total number of parameters refined.
$w = 1/[\sigma^2({F_0}^2) + (aP)^2 + bP\,]$; $P = [2{F_c}^2 + \max({F_0}^2,0)]/3$.

Table S2. Comparison of bimane scaffold bond lengths (Å) in the crystal structures of *syn*-(Me,Me)bimane at room temperature and 100 K.*

Bond		Room temperature (previous literature)[15]	100 K (this work)
C=O	C1–O1	1.217(4)	1.211(5)
	C6–O2	1.207(4)	1.215(5)
OC–C	C1–C2	1.448(4)	1.456(5)
	C5–C6	1.432(4)	1.450(5)
C=C	C2–C3	1.375(4)	1.359(5)
	C4–C5	1.361(4)	1.356(5)
OC–N	C1–N1	1.410(4)	1.403(5)
	C6–N1	1.423(4)	1.415(5)
CC–N	C3–N2	1.361(4)	1.380(5)
	C4–N2	1.372(4)	1.394(5)
N–N	N1–N2	1.378(4)	1.372(3)

* Atom numbering is identical in both structures. Due to the inherent symmetry of the bimane molecule, each bond length in the room-temperature structure can be compared with either of the two corresponding bond lengths in the low-temperature structure.

X-ray crystallographic analysis of complex 2. Diffraction-quality crystals of complex **2** were grown at room temperature from a chloroform solution overlaid with diethyl ether. The crystal parameters are listed in Table S1, and the crystal structure of the complex is depicted in Figures S17 and S18. Select bond lengths are given in Tables S3 and S4. For comparative purposes, Table S3 also contains data for the low-temperature structure of *syn*-(Me,Me)bimane.

A crystal of **2** was also isolated from THF/Et_2O, and identified by its lattice parameters.

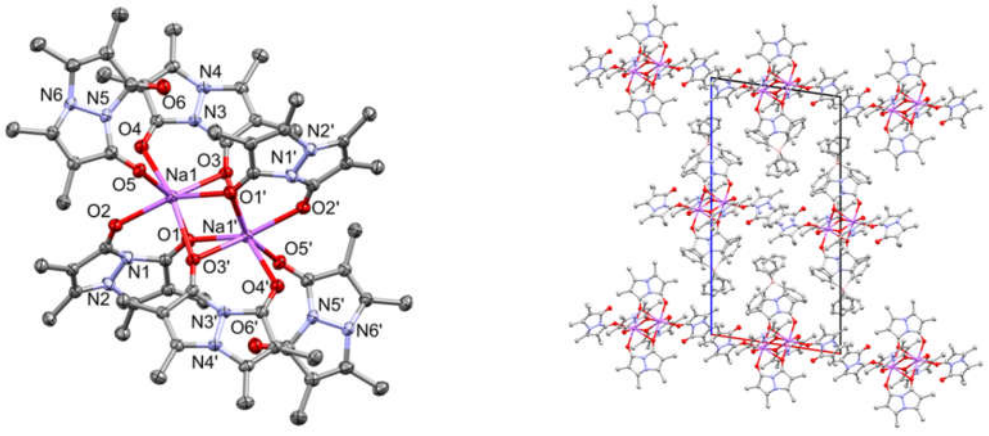

(a) (b)

Figure S17. Crystal structure of complex **2** (with thermal ellipsoids at the 50% probability level): (a) dicationic fragment; (b) unit cell, viewed along the *b* axis. Hydrogen atoms were omitted for clarity. Atoms are color-coded as follows: Na, magenta; O, red; C, grey; N, light blue; B, peach.

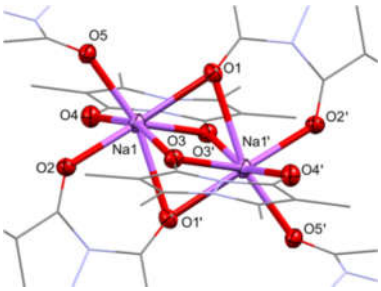

(a)

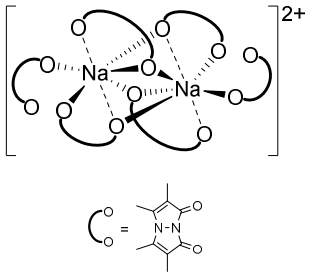

(b)

Figure S18. First coordination sphere of complex **2**: (a) crystal structure (with thermal ellipsoids at the 50% probability level); (b) schematic representation.

Table S3. Bimane scaffold bond lengths (Å) for symmetry-independent bonds in complexes **2**-**4** in comparison with uncoordinated *syn*-(Me,Me)bimane.

Bond	Complex 2	Complex 3	Complex 4 (polymorph A)	Complex 4 (polymorph B)	Total average for complexes*	*syn*-(Me,Me)bimane
C=O	1.2101(19) 1.2147(19) 1.2177(18) 1.2198(18) 1.2253(18) 1.2299(18)	1.188(11) 1.191(10) 1.215(10) 1.219(11) 1.224(11) 1.224(10) 1.234(10) 1.250(11)	1.2246(15) 1.2266(15)	1.2262(14) 1.2275(15)	1.220 ± 0.015	1.211(5) 1.215(5)
OC–C	1.444(2) 1.444(2) 1.450(2) 1.453(2) 1.453(2) 1.460(2)	1.407(11) 1.429(12) 1.437(10) 1.439(13) 1.439(13) 1.450(12) 1.453(12) 1.514(12)	1.4453(17) 1.4498(17)	1.4463(17) 1.4464(17)	1.448 ± 0.022	1.456(5) 1.450(5)
C=C	1.349(2) 1.349(2) 1.357(2) 1.361(2) 1.362(2) 1.366(2)	1.272(15) 1.331(14) 1.343(13) 1.345(12) 1.349(12) 1.354(12) 1.378(13) 1.423(13)	1.3608(17) 1.3632(17)	1.3615(17) 1.3641(17)	1.354 ± 0.030	1.359(5) 1.356(5)
OC–N**	1.4072(19) 1.418(2) 1.3991(19) 1.4038(19)	1.414(10) 1.412(9)	1.4046(15) 1.4069(15)	1.4026(15) 1.4052(15)	1.408 ± 0.006	1.403(5) 1.415(5)
CC–N**	1.382(2) 1.3850(19) 1.3919(19) 1.394(2)	1.343(11) 1.394(11)	1.3921(15) 1.3923(15)	1.3906(15) 1.3920(15)	1.384 ± 0.017	1.380(5) 1.394(5)
N–N**	1.3856(17) 1.3719(18)	1.413(10)	1.3711(13)	1.3730(13)	1.383 ± 0.018	1.372(3)

* Averaging excludes polymorph B of complex **4**.

** Complexes **2** and **3** are disordered at bimane nitrogen atoms. This table only includes bond lengths that are associated with non-disordered nitrogen atoms.

Table S4. Na–O bond lengths (Å) for symmetry-independent bonds in complexes **2**-**4**.				
Complex 2	**Complex 3**	**Complex 4 (polymorph A)**	**Complex 4 (polymorph B)**	**Total average***
2.3293(12) 2.3600(12) 2.4295(12) 2.4798(12) 2.5200(12) 2.5335(12) 2.7031(12)	2.364(7) 2.372(7) 2.378(7) 2.381(7) 2.388(6) 2.407(7) 2.408(7) 2.436(8) 2.461(7) 2.485(7)	2.2902(9) 2.3138(10)	2.2894(9) 2.3127(10)	2.42 ± 0.10

* Averaging excludes polymorph B of complex **4**.

X-ray crystallographic analysis of complex 3. Crystals of complex **3** suitable for X-ray diffraction were grown at 4 °C from an acetonitrile solution overlaid with diethyl ether. The crystal parameters are given in Table S1, and the crystal structure of the complex is shown in Figures S19 and S20. Select bond lengths are collected in Tables S3 and S4. For comparative purposes, Table S3 also contains data for the low-temperature structure of *syn*-(Me,Me)bimane.

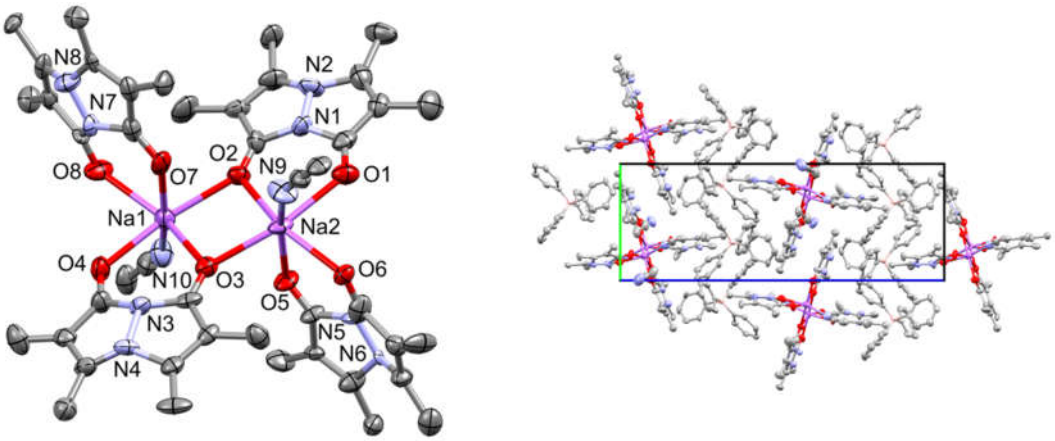

(a) (b)

Figure S19. Crystal structure of complex **3** (with thermal ellipsoids at the 50% probability level): (a) dicationic fragment; (b) unit cell, viewed along the *a* axis. Hydrogen atoms were omitted for clarity. Atoms are color-coded as follows: Na, magenta; O, red; C, grey; N, light blue; B, peach.

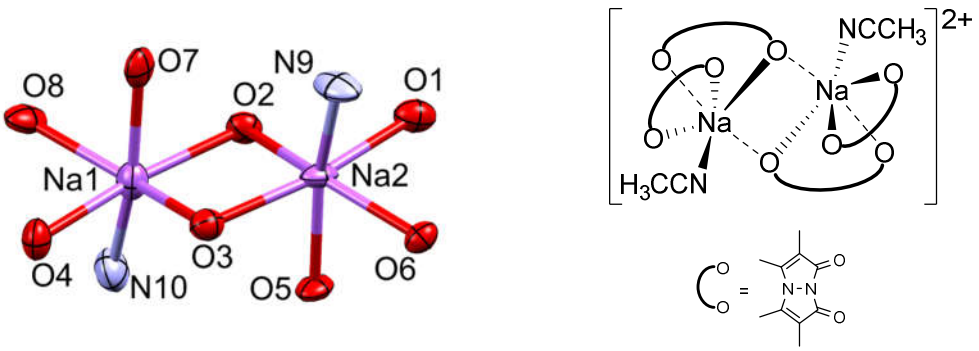

(a) (b)

Figure S20. First coordination sphere of complex **3**: (a) crystal structure (with thermal ellipsoids at the 50% probability level); (b) schematic representation.

X-ray crystallographic analysis of complex 4. Diffraction-quality crystals of complex **4** were grown at room temperature from a chloroform solution overlaid with diethyl ether. The crystal parameters are listed in Table S1, and the crystal structure of the complex is depicted in Figure S21. Select bond lengths are given in Tables S3 and S4. For comparative purposes, Table S3 also contains data for the low-temperature structure of *syn*-(Me,Me)bimane.

A second crystal of complex **4** was isolated from a chloroform solution overlaid with diethyl ether, which was kept at 4 °C instead of room temperature. This crystal was found to be a polymorph of the aforementioned structure, belonging to the same monoclinic *C2/c* space group. It also has virtually identical lattice parameters, except for the lattice constant *c* (20.91 instead of 19.09 Å) and angle *β* (121.3 instead of 110.4°). The two polymorphs - A and B, respectively - have essentially identical structural metrics, as can be seen in Tables S3 and S4.

A second crystal of polymorph A of complex **4** was also isolated from C_6H_5F/Et_2O, and identified by its lattice parameters.

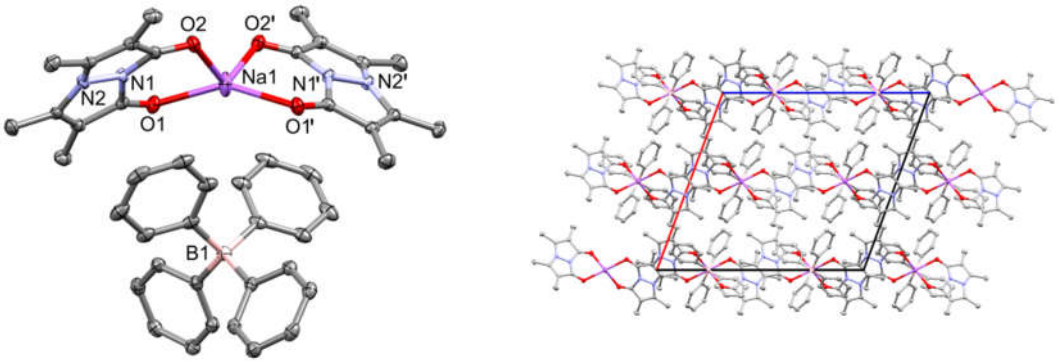

(a) (b)

Figure S21. Crystal structure of complex **4** (with thermal ellipsoids at the 50% probability level): (a) cationic fragment; (b) unit cell, viewed along the *b* axis. Hydrogen atoms were omitted for clarity. Atoms are color-coded as follows: Na, magenta; O, red; C, grey; N, light blue; B, peach.

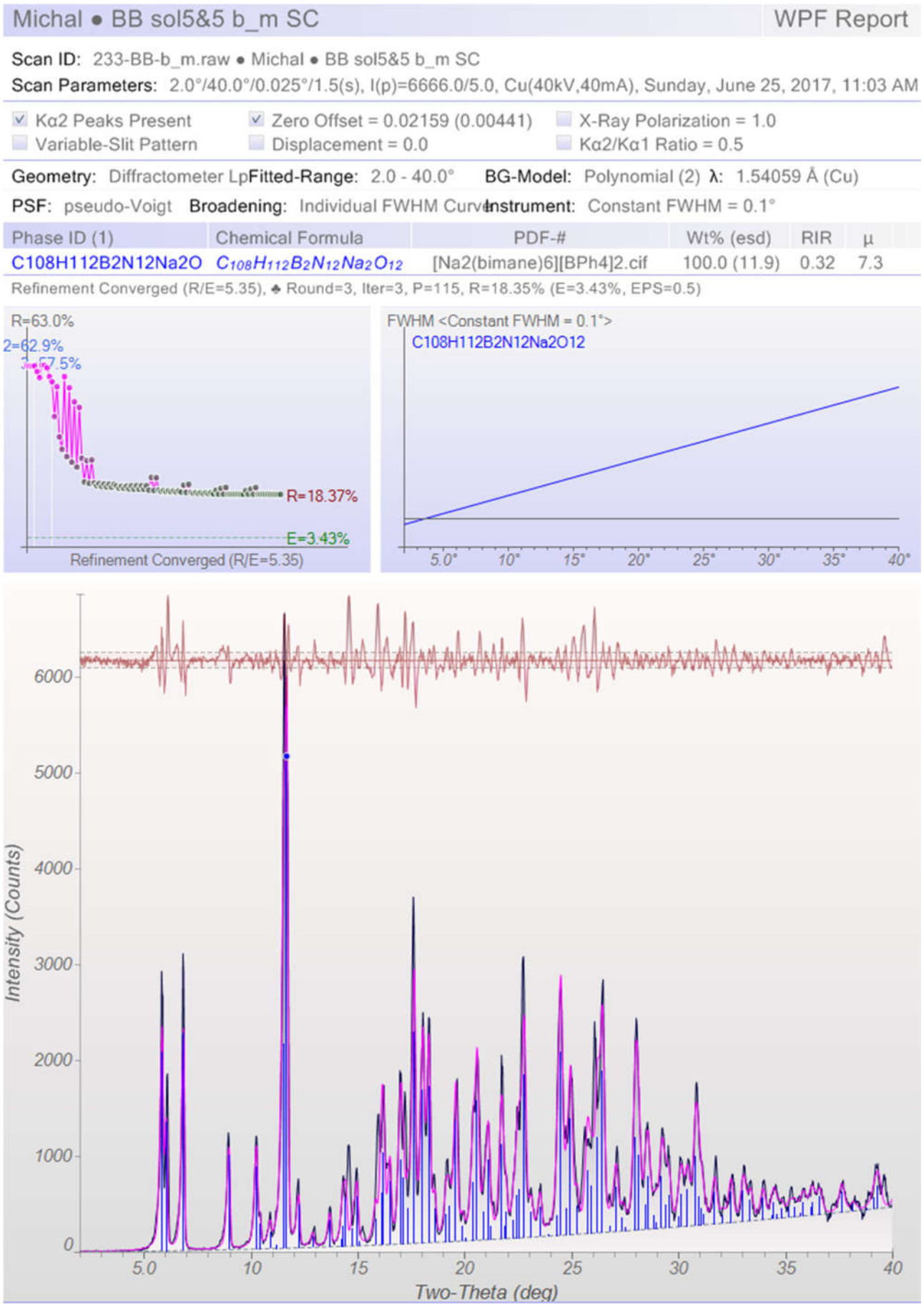

Figure S22. Powder X-ray diffraction data for complex **2**.

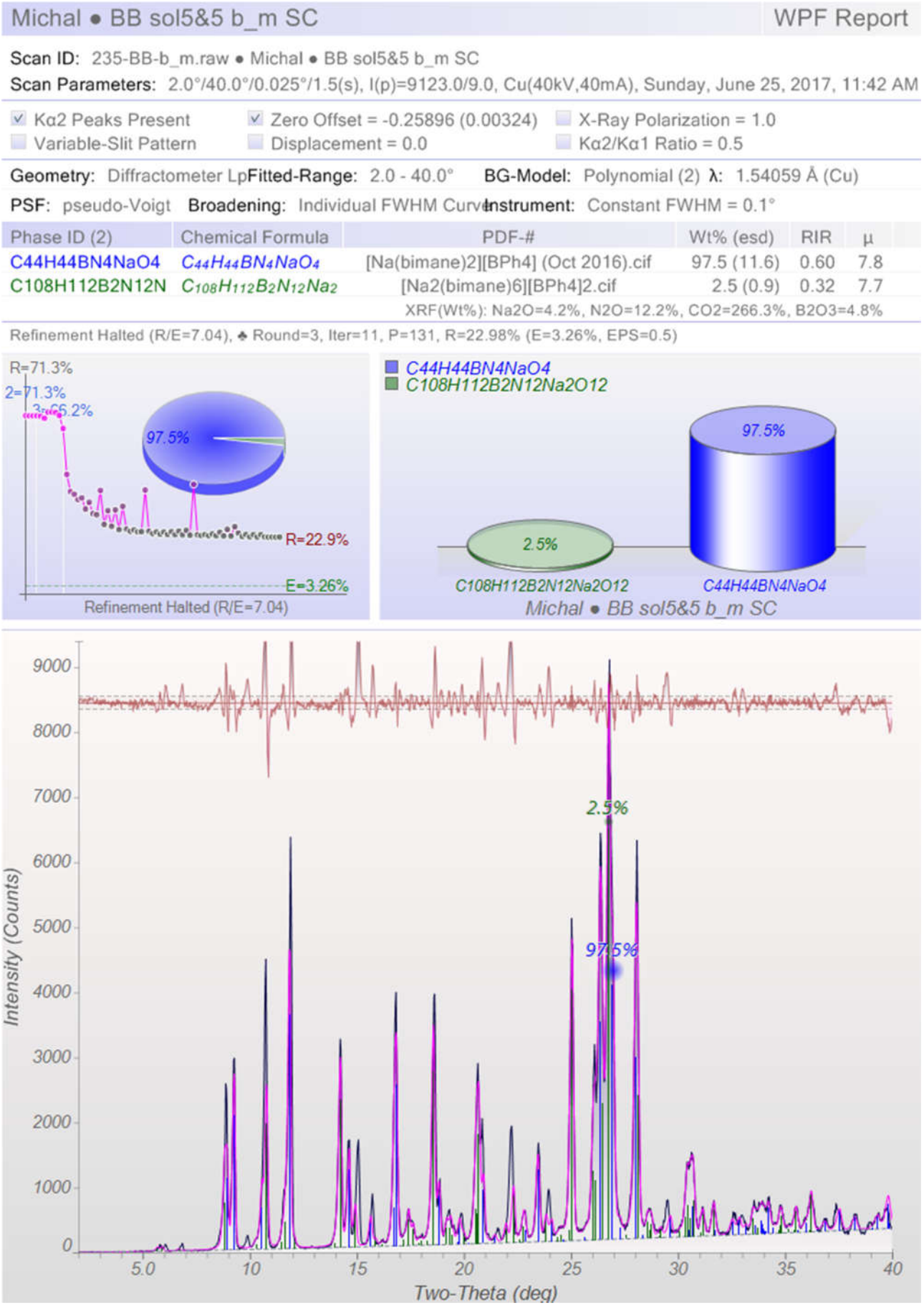

Figure S23. Powder X-ray diffraction data for complex **4**. The sample also contains 2.5% of complex **2**.

Table S5. Maximal absorbance at the n→π* band (A_{max}) and maximal fluorescence intensity (I_F)* for 1 mM *syn*-(Me,Me)bimane in the presence of varying concentrations of $NaBPh_4$ in $CHCl_3$, THF, CH_3CN and H_2O. A_{max} and I_F are in %, relative to their values in the absence of the salt. Each value is averaged over the cited number of samples, and the standard deviation is given in parentheses.

Solvent	[$NaBPh_4$] (mM)	Number of samples	A_{max}	I_F* (uncorrected)	I_F* (Absorbance-corrected)
$CHCl_3$	0.10	3	95(3)	87(10)	91(8)
	0.20	3	99(5)	83(8)	84(12)
	0.33	3	97(5)	74(6)	76(7)
	0.50	4	91(3)	57(5)	62(4)
THF	0.10	4	97(1)	93(2)	96(2)
	0.25	4	95(2)	84(2)	89(2)
	0.33	4	93(4)	76(2)	81(3)
	0.50	4	89(3)	65(1)	72(2)
	1.0	4	85(4)	47(4)	54(4)
	3.0	8	79(4)	26(6)	31(7)
	5.0	4	78(5)	13(2)	16(2)
	10.0	5	75(2)	8(1)	10(2)
CH_3CN	0.50	3	96(5)	91(2)	94(2)
	3.0	3	96(8)	82(1)	86(6)
	10.0	3	99(2)	65(7)	67(7)
H_2O	0.50	4	96(9)	94(3)	99(7)
	1.0	3	97(4)	88(4)	92(5)
	3.0	3	98(7)	78(7)	80(2)
	5.0	4	94(6)	64(5)	68(2)
	10.0	5	98(3)	53(4)	55(5)

* λ_{ex} (nm): $CHCl_3$, 370; THF, 370; CH_3CN, 370; H_2O, 380.

Table S6. Wavelengths at maximal absorbance of the n→π* band (λ_{max}) and maximal fluorescence emission (λ_{em}) for 1 mM *syn*-(Me,Me)bimane in the presence of varying concentrations of $NaBPh_4$ in $CHCl_3$, THF, CH_3CN and H_2O. All wavelengths are in nm. Each value is averaged over the cited number of samples, and the standard deviation is given in parentheses.

Solvent	**[$NaBPh_4$] (mM)**	**Number of samples**	**λ_{max}**	**λ_{em}**
$CHCl_3$	0.00	4	368(2)	429(1)
	0.10	3	368.3(6)	429.7(6)
	0.33	3	369(3)	430(2)
	0.50	4	371(1)	429.5(6)
THF	0.00	9	361(1)	421(2)
	0.10	4	361.3(5)	420.5(6)
	0.25	4	362(2)	420(2)
	0.33	4	363(1)	421(1)
	0.50	4	364.0(8)	422(2)
	1.0	4	366(2)	423.0(8)
	3.0	8	369(1)	428(5)
	5.0	4	372(2)	433(6)
	10.0	5	373(1)	437(4)
CH_3CN	0.00	4	369(2)	434(1)
	0.50	3	369(1)	433.0(5)
	3.0	3	369.7(6)	434(1)
	10.0	4	371(2)	436(1)
H_2O	0.00	5	388(2)	476(1)
	0.50	4	387.0(8)	477(2)
	1.0	3	388(2)	477(2)
	3.0	3	388(2)	476(2)
	5.0	4	387(1)	477(2)
	10.0	4	388(1)	477(2)

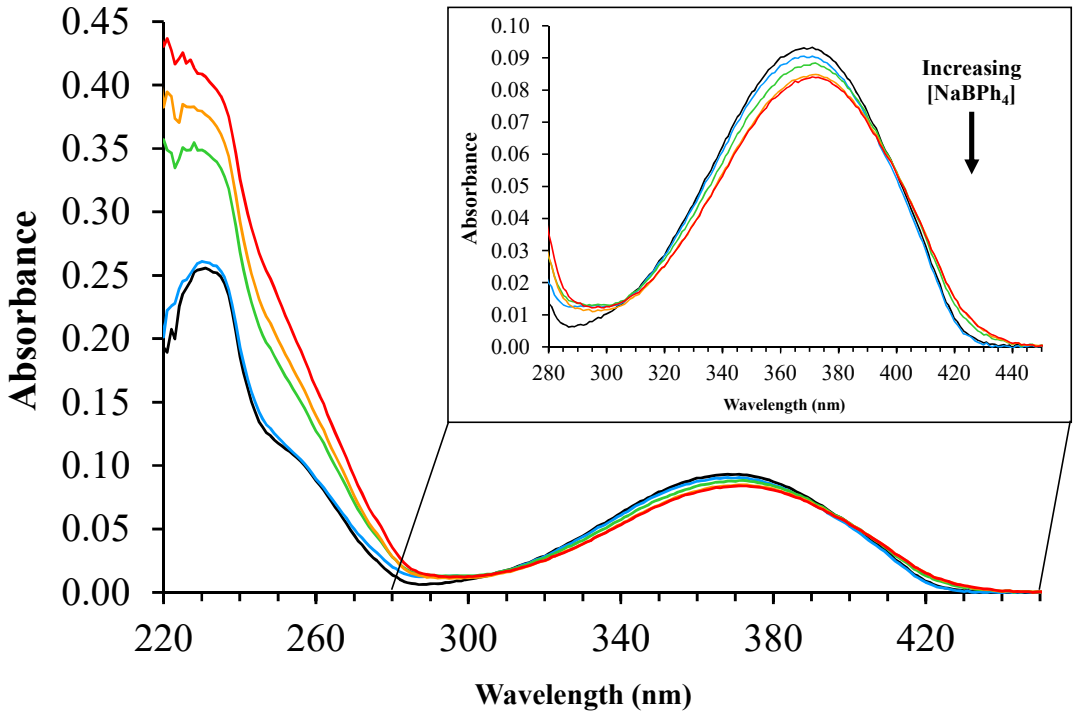

Figure S24. UV-Vis absorbance spectra of 1 mM *syn*-(Me,Me)bimane in $CHCl_3$, in the presence of increasing concentrations of $NaBPh_4$. The plots correspond to [$NaBPh_4$] = 0, 0.10, 0.25, 0.33, 0.50 mM. The optical pathlength was 0.1 mm.

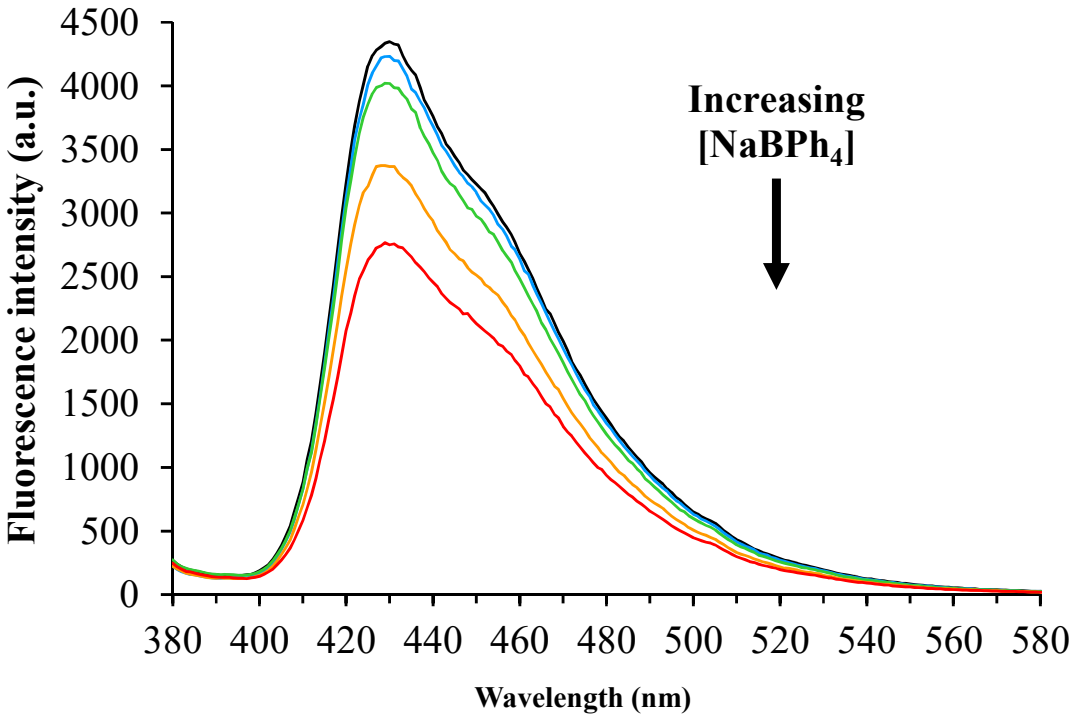

Figure S25. Fluorescence emission spectra of 1 mM *syn*-(Me,Me)bimane in $CHCl_3$, in the presence of increasing concentrations of $NaBPh_4$ (λ_{ex} = 370 nm). The plots correspond to [$NaBPh_4$] = 0, 0.10, 0.25, 0.33, 0.50 mM.

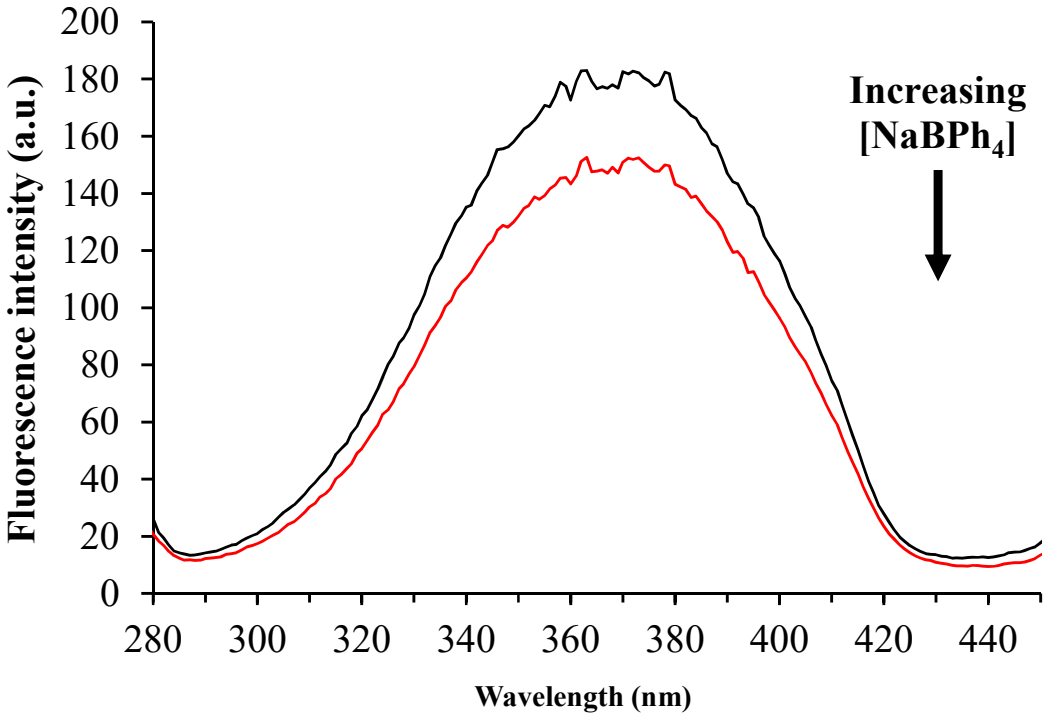

Figure S26. Fluorescence excitation spectra of 1 mM *syn*-(Me,Me)bimane in $CHCl_3$, in the absence and presence of $NaBPh_4$ (λ_{em} = 480 nm). The plots correspond to [$NaBPh_4$] = 0, 0.50 mM. Only the n→π* band is shown.

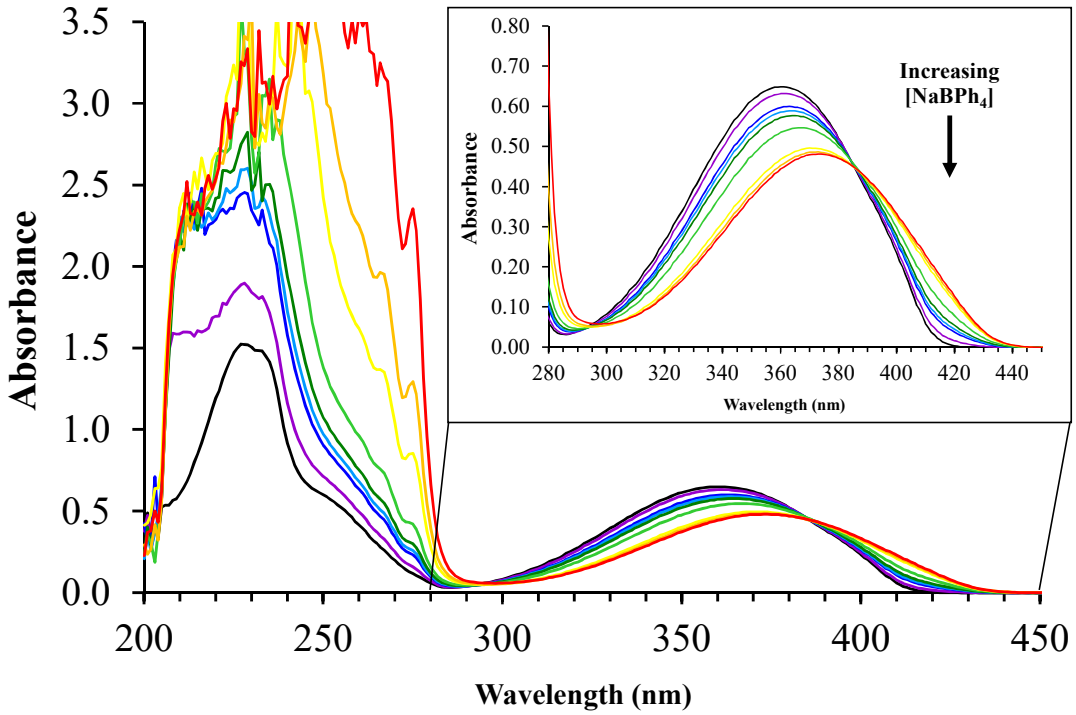

Figure S27. UV-Vis absorbance spectra of 1 mM *syn*-(Me,Me)bimane in THF, in the presence of increasing concentrations of $NaBPh_4$. The plots correspond to [$NaBPh_4$] = 0, 0.10, 0.25, 0.33, 0.50, 1.0, 3.0, 5.0, 10.0 mM.

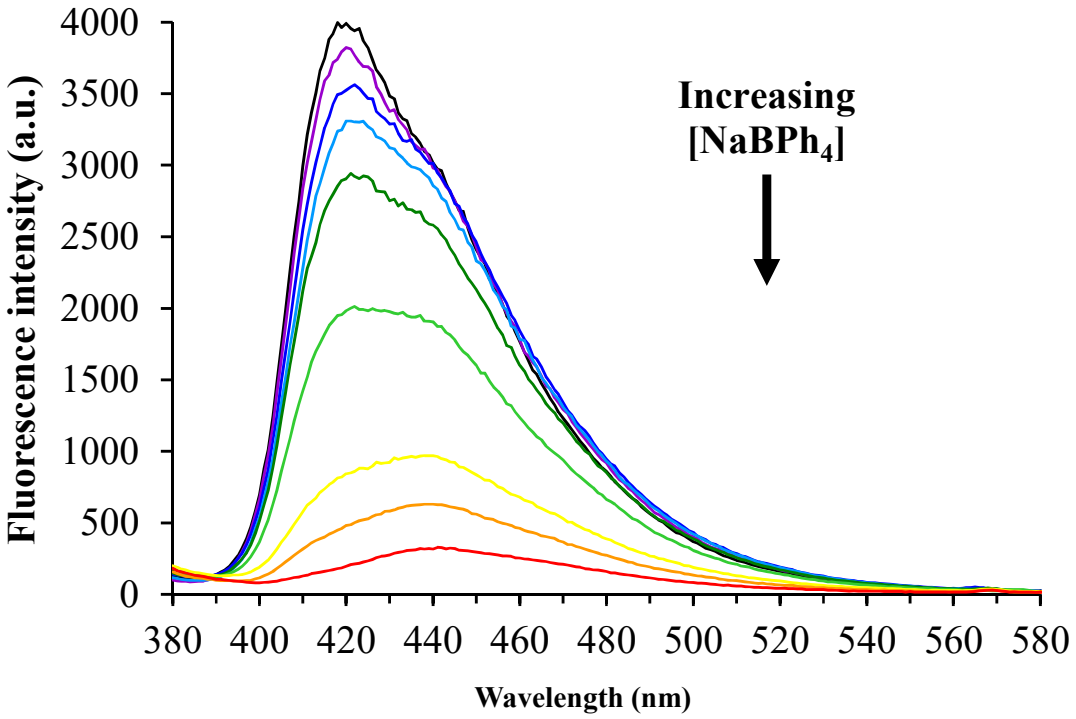

Figure S28. Fluorescence emission spectra of 1 mM *syn*-(Me,Me)bimane in THF, in the presence of increasing concentrations of $NaBPh_4$ (λ_{ex} = 360 nm). The plots correspond to [$NaBPh_4$] = 0, 0.10, 0.25, 0.33, 0.50, 1.0, 3.0, 5.0, 10.0 mM.

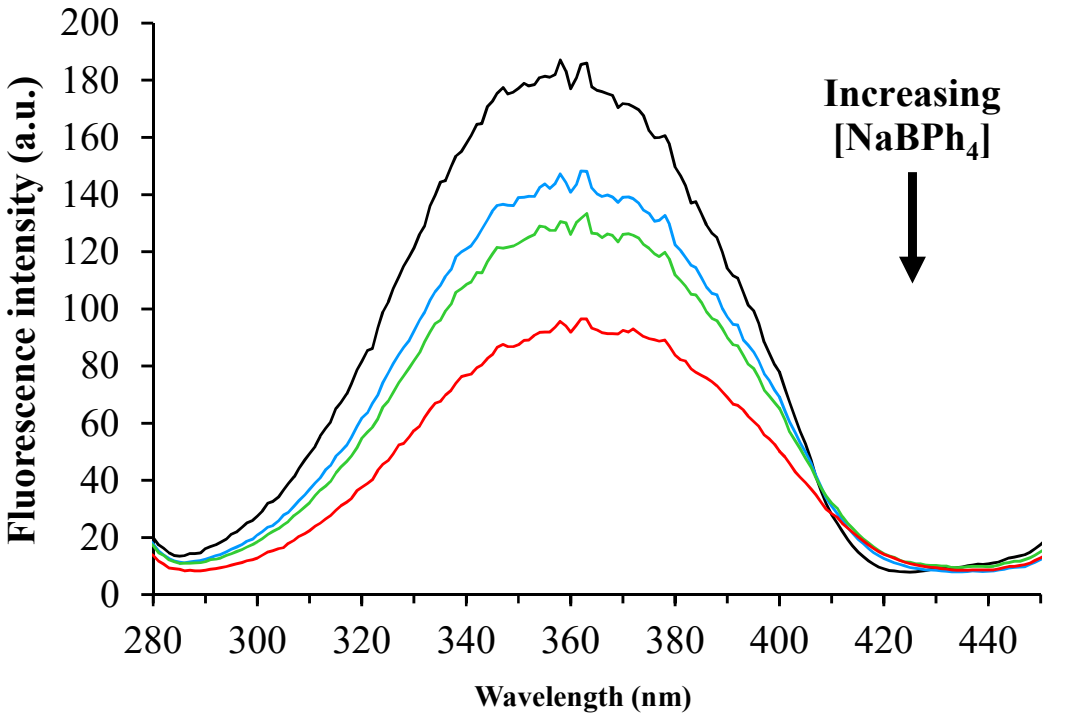

Figure S29. Fluorescence excitation spectra of 1 mM *syn*-(Me,Me)bimane in THF, in the presence of increasing concentrations of $NaBPh_4$ (λ_{em} = 475 nm). The plots correspond to [$NaBPh_4$] = 0, 0.33, 0.50, 1.0 mM. Only the n→π* band is shown.

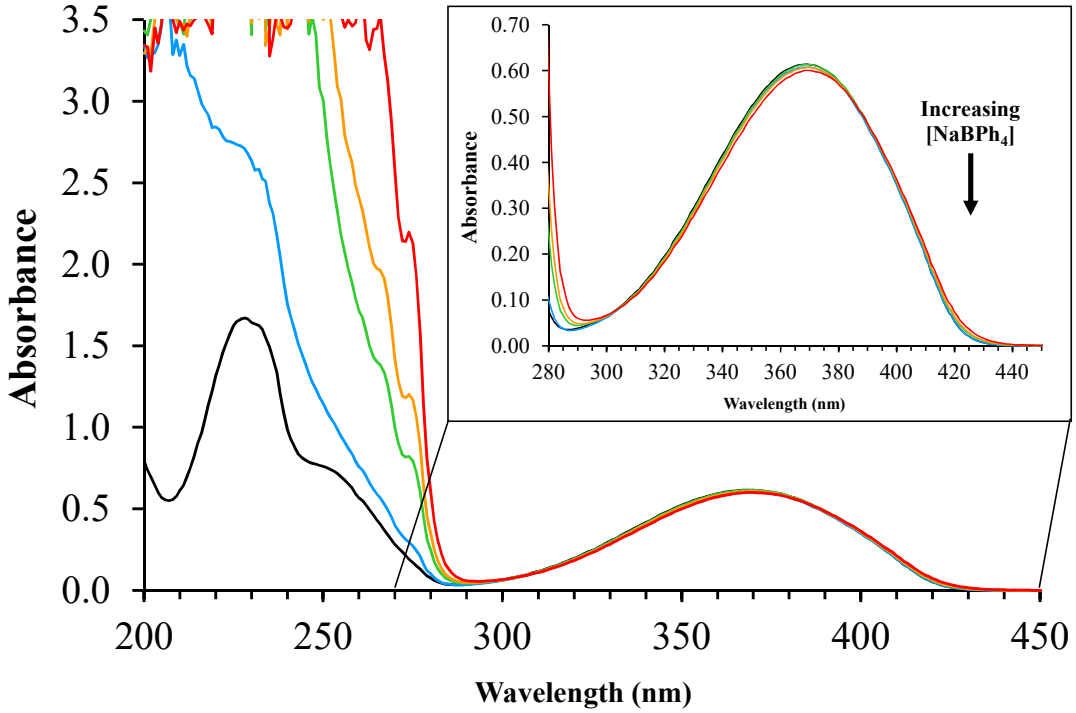

Figure S30. UV-Vis absorbance spectra of 1 mM *syn*-(Me,Me)bimane in CH_3CN, in the presence of increasing concentrations of $NaBPh_4$. The plots correspond to [$NaBPh_4$] = 0, 0.50, 3.0, 5.0, 10.0 mM.

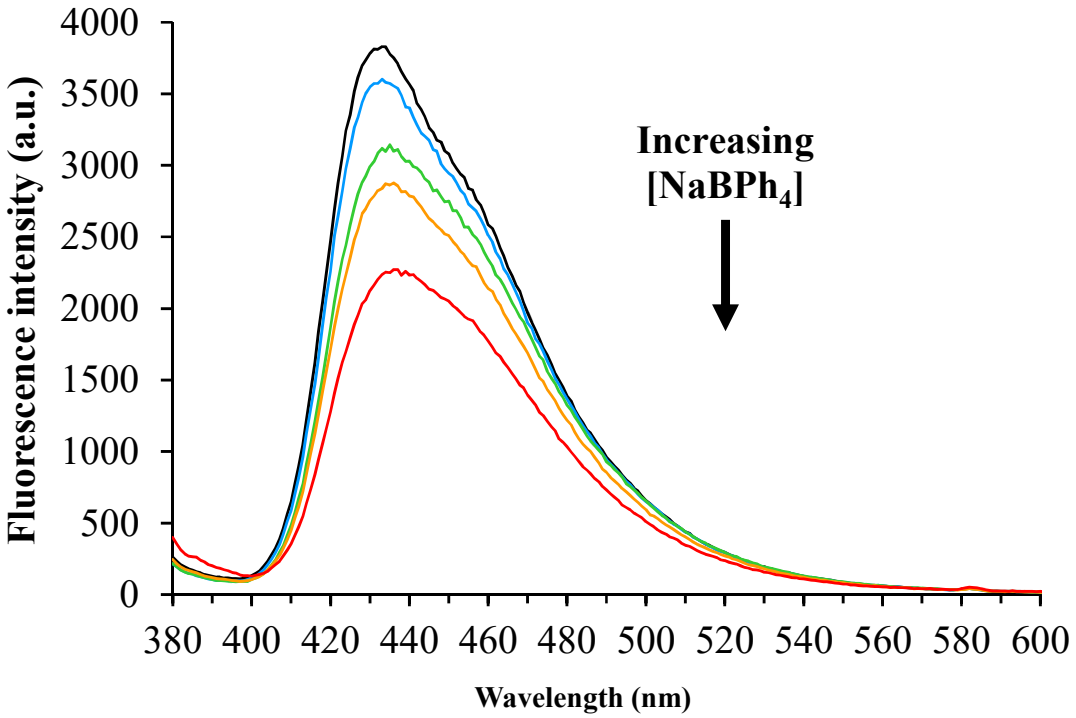

Figure S31. Fluorescence emission spectra of 1 mM *syn*-(Me,Me)bimane in CH_3CN, in the presence of increasing concentrations of $NaBPh_4$ (λ_{ex} = 369 nm). The plots correspond to [$NaBPh_4$] = 0, 0.50, 3.0, 5.0, 10.0 mM.

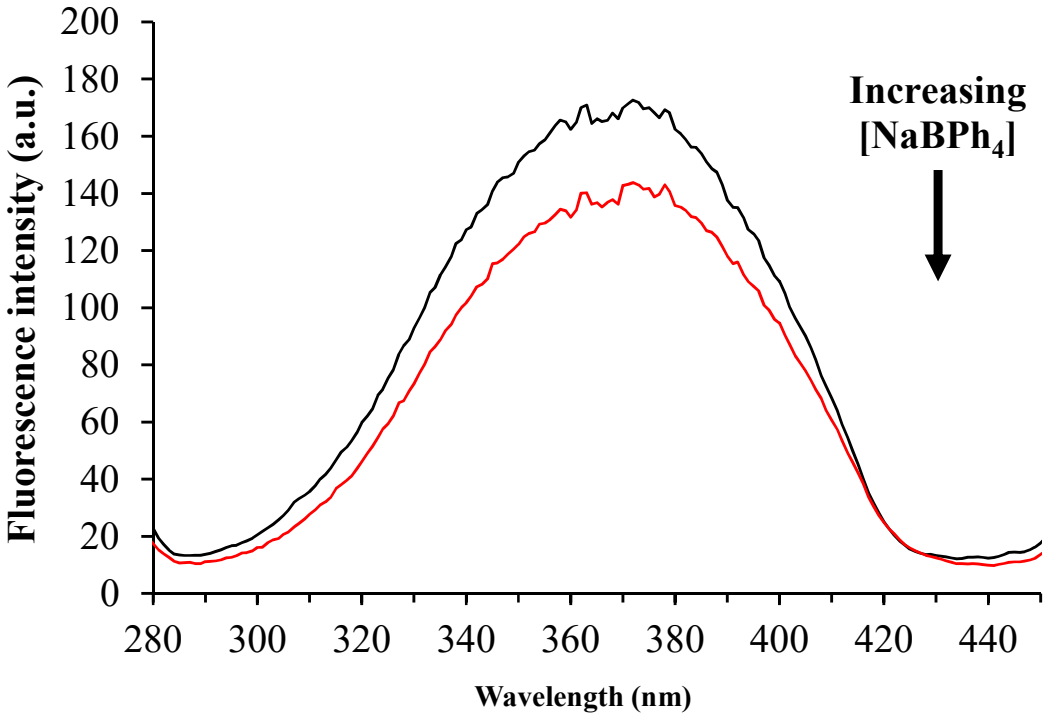

Figure S32. Fluorescence excitation spectra of 1 mM *syn*-(Me,Me)bimane in CH_3CN, in the absence and presence of $NaBPh_4$ (λ_{em} = 485 nm). The plots correspond to [$NaBPh_4$] = 0, 10.0 mM. Only the n→π* band is shown.

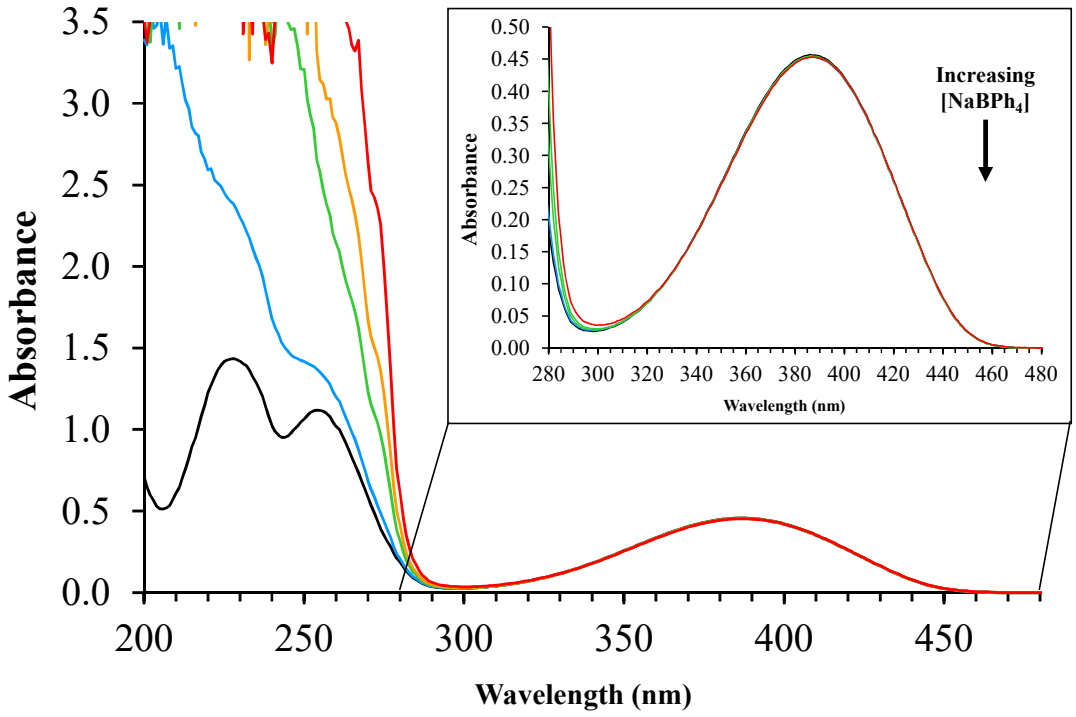

Figure S33. UV-Vis absorbance spectra of 1 mM *syn*-(Me,Me)bimane in H_2O, in the presence of increasing concentrations of $NaBPh_4$. The plots correspond to [$NaBPh_4$] = 0, 0.50, 3.0, 5.0, 10.0 mM.

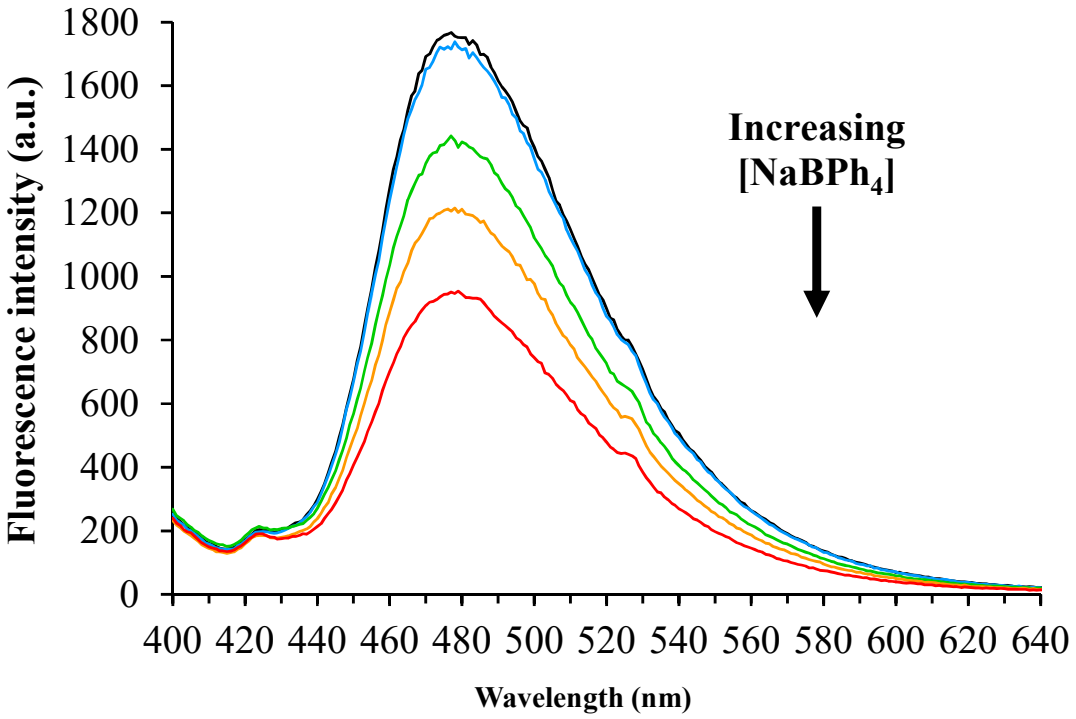

Figure S34. Fluorescence emission spectra of 1 mM *syn*-(Me,Me)bimane in H_2O, in the presence of increasing concentrations of $NaBPh_4$ (λ_{ex} = 390 nm). The plots correspond to [$NaBPh_4$] = 0, 0.50, 3.0, 5.0, 10.0 mM.

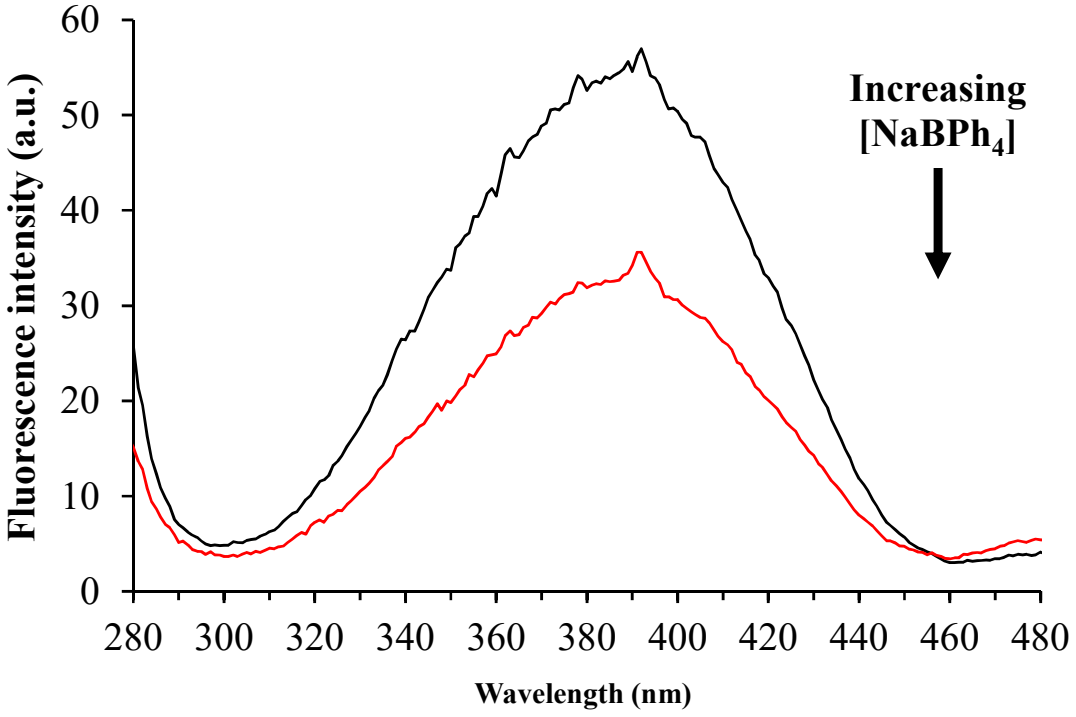

Figure S35. Fluorescence excitation spectra of 1 mM *syn*-(Me,Me)bimane in H_2O, in the absence and presence of $NaBPh_4$ (λ_{em} = 535 nm). The plots correspond to [$NaBPh_4$] = 0, 10.0 mM. Only the n→π* band is shown.

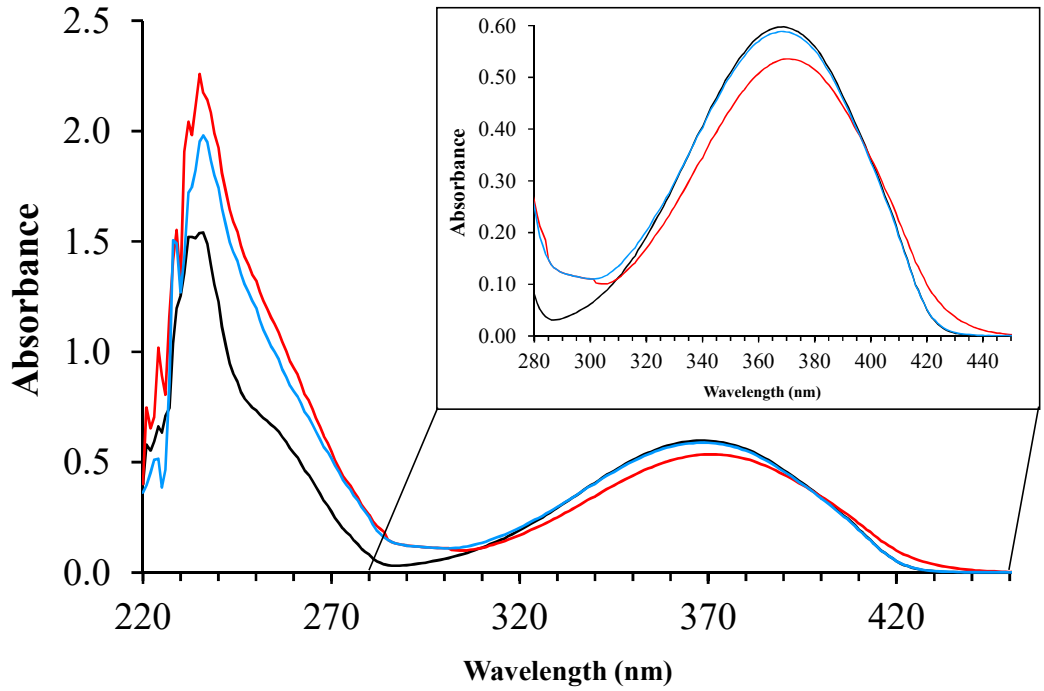

Figure S36. UV-Vis absorbance spectra of 1 mM *syn*-(Me,Me)bimane in $CHCl_3$, in the absence and presence of $NaBPh_4$, and after addition of 18-crown-6 to the sodium-containing mixture: (a) black, no added $NaBPh_4$; (b) red, 0.5 mM $NaBPh_4$; (c) blue, 0.5 mM $NaBPh_4$ + 0.75 mM 18-crown-6. The blue and black plots overlap.

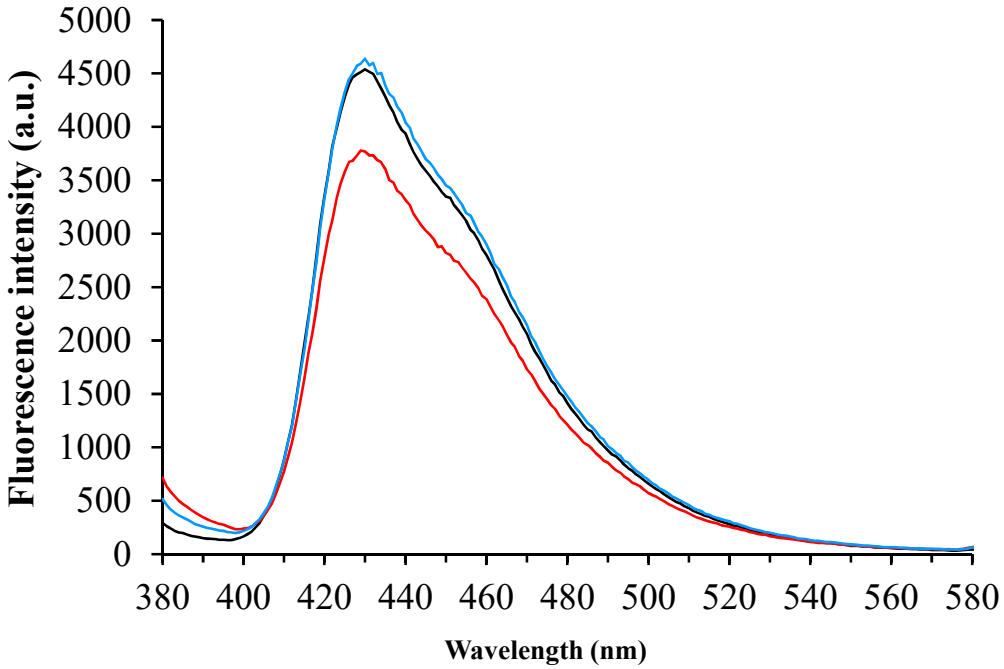

Figure S37. Fluorescence emission spectra of 1 mM *syn*-(Me,Me)bimane in $CHCl_3$ (λ_{ex} = 368 nm), in the absence and presence of $NaBPh_4$, and after addition of 18-crown-6 to the sodium-containing mixture: (a) black, no added $NaBPh_4$; (b) red, 0.5 mM $NaBPh_4$; (c) blue, 0.5 mM $NaBPh_4$ + 0.75 mM 18-crown-6. The blue and black plots partly overlap.

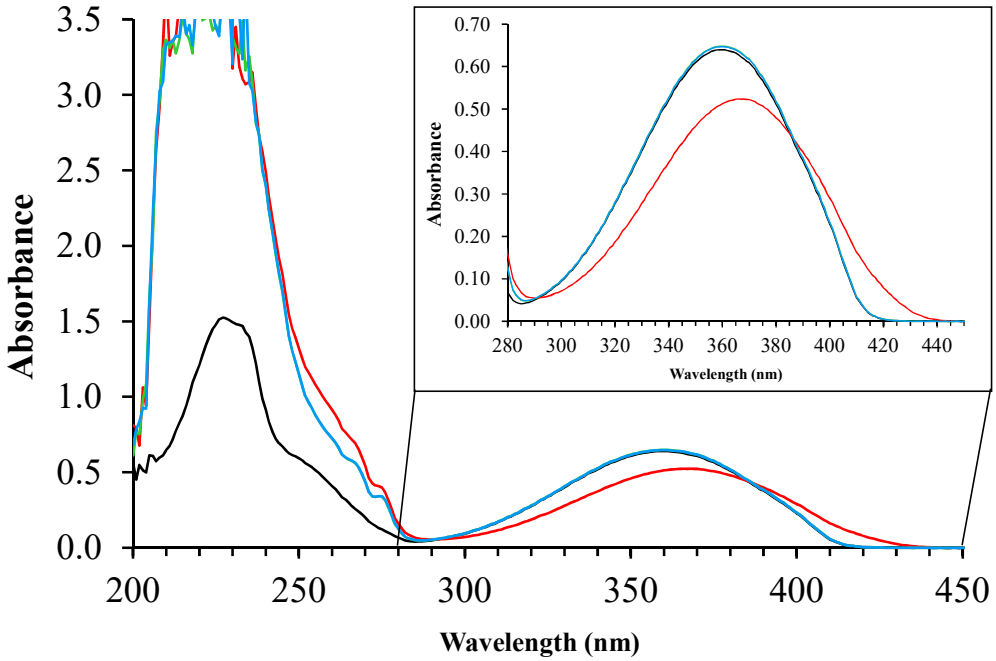

Figure S38. UV-Vis absorbance spectra of 1 mM *syn*-(Me,Me)bimane in THF, in the absence and presence of $NaBPh_4$, and after addition of 18-crown-6 to the sodium-containing mixture: (a) black, no added $NaBPh_4$; (b) red, 1 mM $NaBPh_4$; (c) green, 1 mM $NaBPh_4$ + 1 mM 18-crown-6; (d) blue, 1 mM $NaBPh_4$ + 2 mM 18-crown-6. The blue, green and black plots overlap.

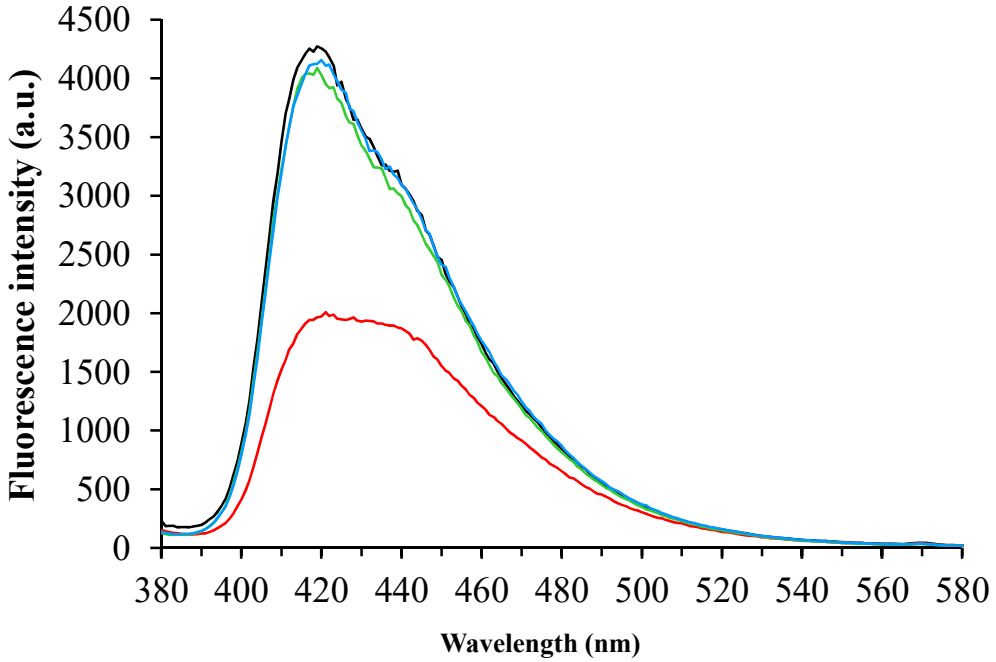

Figure S39. Fluorescence emission spectra of 1 mM *syn*-(Me,Me)bimane in THF (λ_{ex} = 361 nm), in the absence and presence of $NaBPh_4$, and after addition of 18-crown-6 to the sodium-containing mixture: (a) black, no added $NaBPh_4$; (b) red, 1 mM $NaBPh_4$; (c) green, 1 mM $NaBPh_4$ + 1 mM 18-crown-6; (d) blue, 1 mM $NaBPh_4$ + 2 mM 18-crown-6. The green, blue and black plots partly overlap.

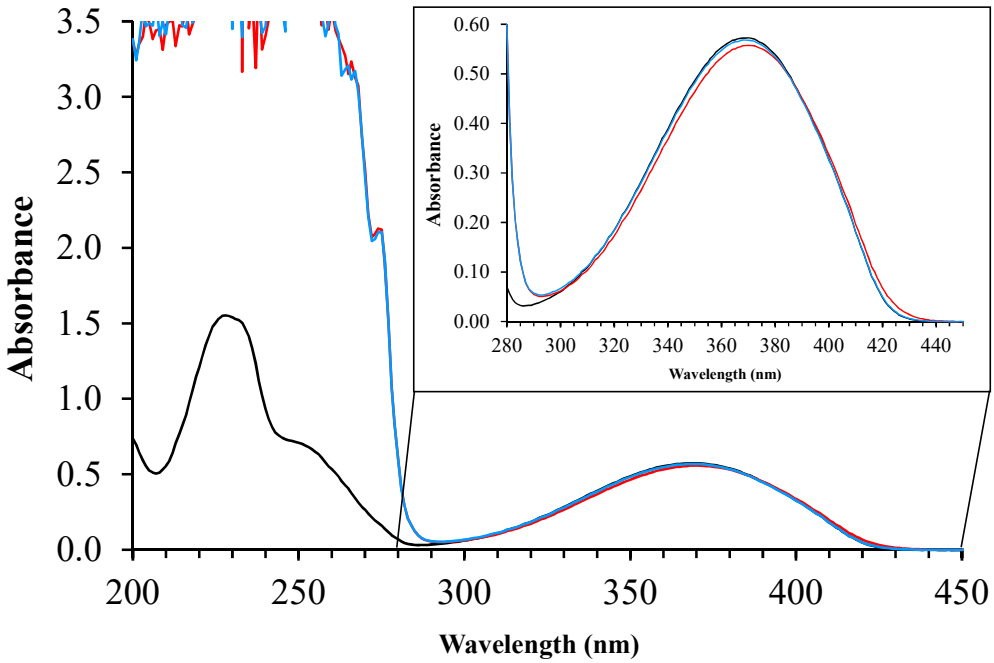

Figure S40. UV-Vis absorbance spectra of 1 mM *syn*-(Me,Me)bimane in CH_3CN, in the absence and presence of $NaBPh_4$, and after addition of 18-crown-6 to the sodium-containing mixture: (a) black, no added $NaBPh_4$; (b) red, 10 mM $NaBPh_4$; (c) blue, 10 mM $NaBPh_4$ + 10 mM 18-crown-6. The blue and black plots overlap.

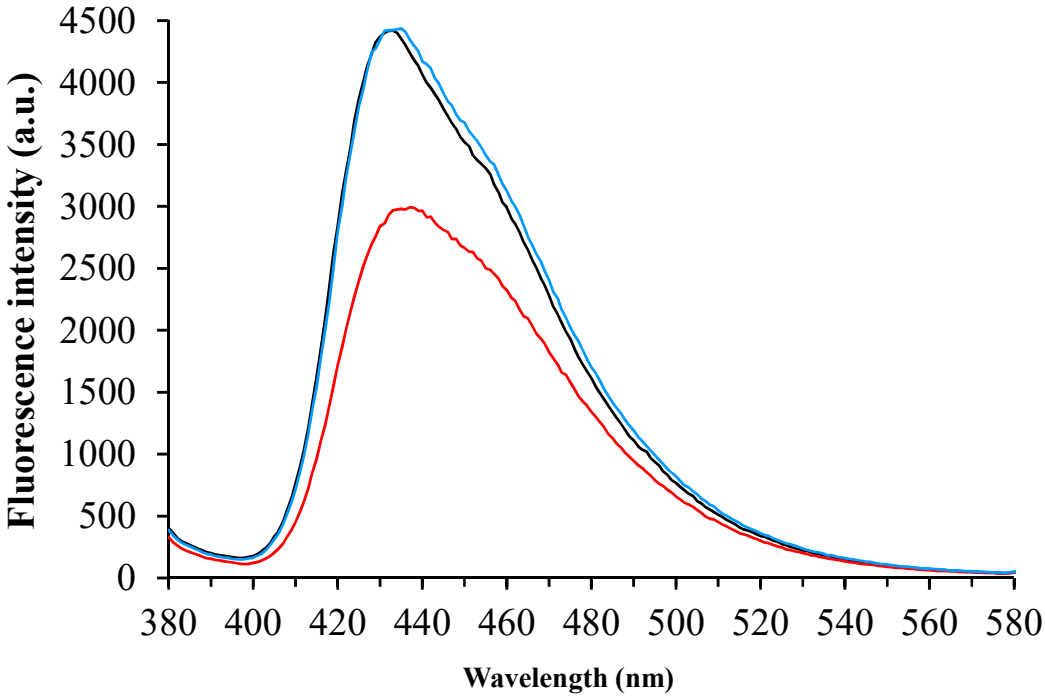

Figure S41. Fluorescence emission spectra of 1 mM *syn*-(Me,Me)bimane in CH_3CN (λ_{ex} = 369 nm), in the absence and presence of $NaBPh_4$, and after addition of 18-crown-6 to the sodium-containing mixture: (a) black, no added $NaBPh_4$; (b) red, 10 mM $NaBPh_4$; (c) blue, 10 mM $NaBPh_4$ + 10 mM 18-crown-6. The blue and black plots partly overlap.

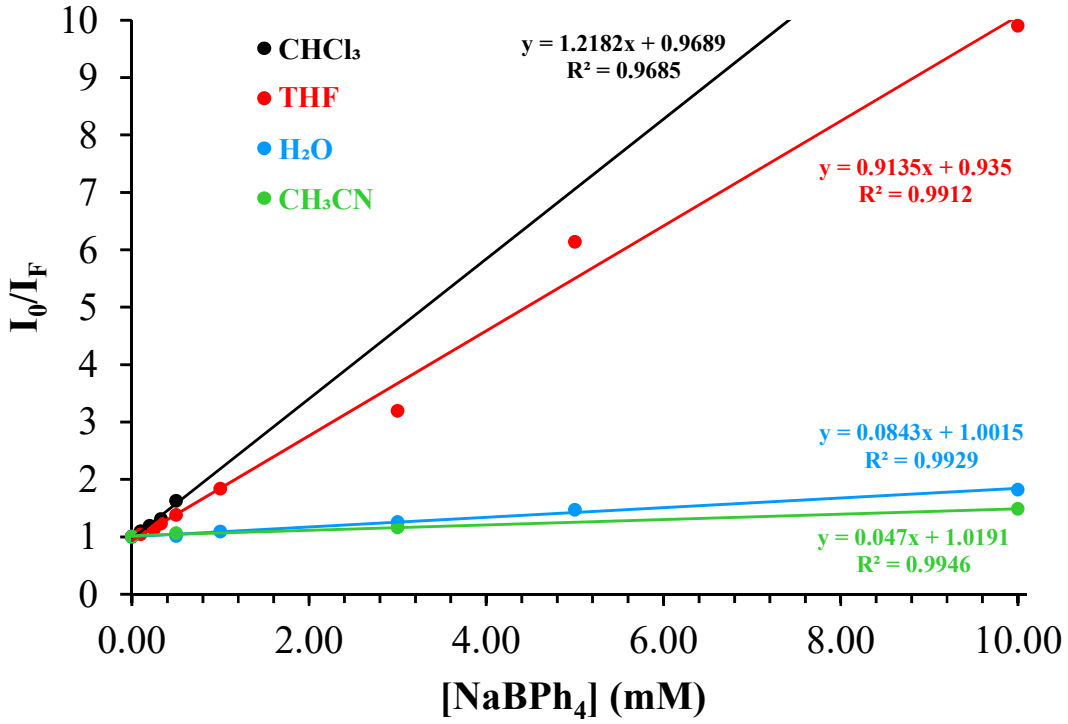

Figure S42. Stern-Volmer plots for the fluorescence quenching of 1 mM *syn*-(Me,Me)bimane by $NaBPh_4$ in $CHCl_3$, THF, CH_3CN and H_2O. The graphs were generated using the absorbance-corrected fluorescence data in Table S5. Each data point in the plots represents an average of at least 3 independent measurements.

Table S7. Maximal absorbance at the n→π* band (A_{max}) and maximal fluorescence intensity (I_F)* for 5 μM *syn*-(Me,Me)bimane in the presence of varying concentrations of $NaBPh_4$ in THF and H_2O. A_{max} and I_F are in %, relative to their values in the absence of the salt. Each value is averaged over the cited number of samples, and the standard deviation is given in parentheses.

Solvent	[$NaBPh_4$] (mM)	Number of samples	A_{max}	I_F* (uncorrected)	I_F* (Absorbance-corrected)
THF	5.0×10^{-3}	3	98(3)	93.8(9)	96(4)
	5.0×10^{-2}	3	92(7)	79.9(2)	87(8)
	0.25	3	90(4)	50(7)	56(6)
	0.50	3	82(6)	32.5(8)	40(4)
	1.0	2	78.2(7)	20.3(5)	25.6(5)
	2.5	2	75(1)	10.1(2)	13.4(6)
	5.0	3	71(6)	5.5(2)	7.7(6)
	7.5	2	72(4)	3.90(5)	5.4(2)
	10.0	3	71(5)	3.08(5)	4.5(6)
H_2O	5.0×10^{-3}	3	100(4)	99.9(4)	100(4)
	5.0×10^{-2}	3	98(4)	99.4(6)	102(3)
	0.25	3	100(3)	97.2(1)	99(3)
	0.50	3	99(2)	94.6(3)	96(1)
	1.0	3	97(5)	91.0(5)	94(5)
	2.5	3	97(7)	79.7(3)	83(5)
	5.0	3	96(7)	63(4)	66(7)
	7.5	3	96(6)	54(1)	57(4)
	10.0	3	97(6)	47.0(9)	49(1)

* λ_{ex} (nm): THF, 370; H_2O, 390.

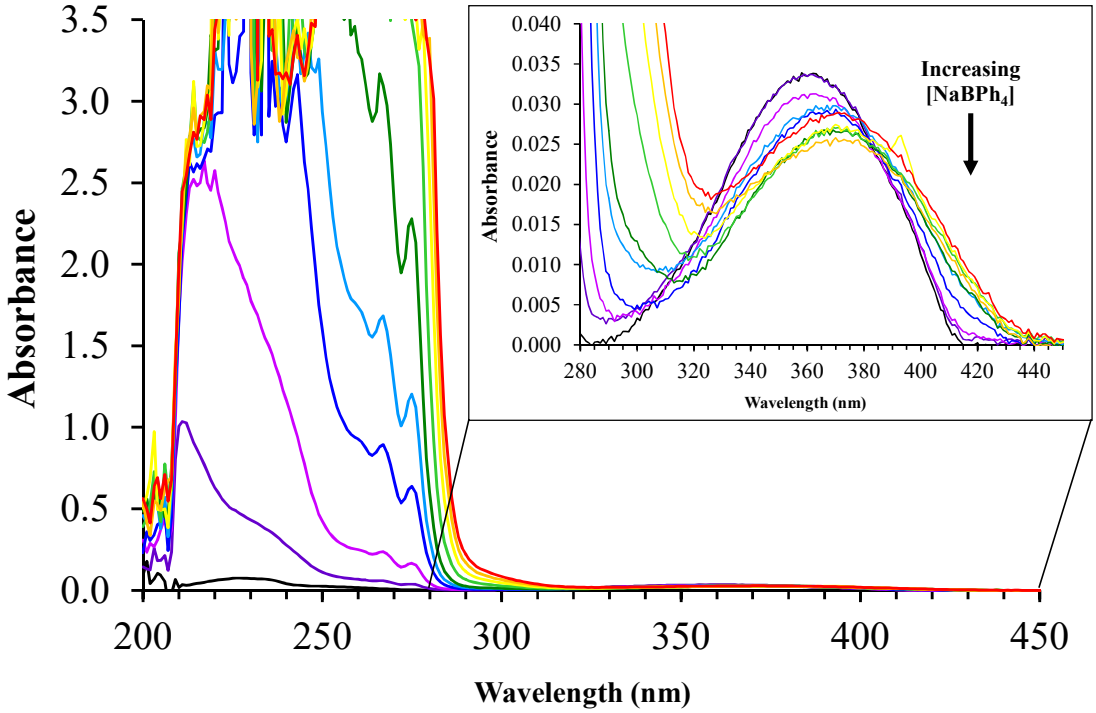

Figure S43. UV-Vis absorbance spectra of 5 μM *syn*-(Me,Me)bimane in THF, in the presence of increasing concentrations of $NaBPh_4$. The plots correspond to [$NaBPh_4$] = 0, 5.0×10^{-3}, 5.0×10^{-2}, 0.25, 0.50, 1.0, 2.5, 5.0, 7.5, 10.0 mM.

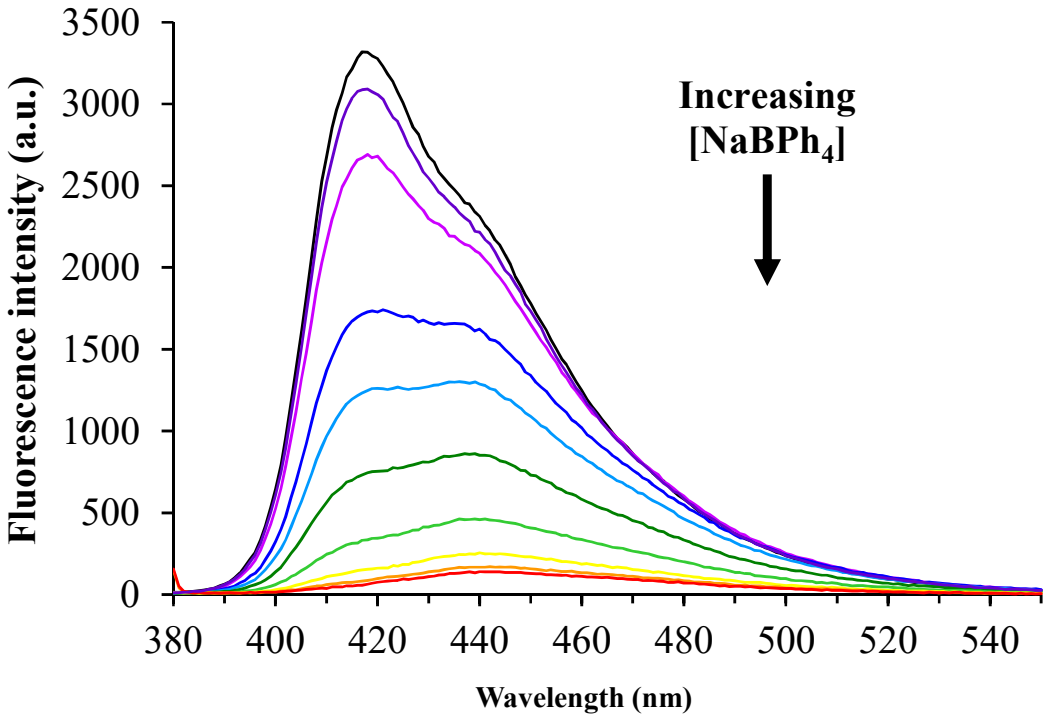

Figure S44. Fluorescence emission spectra of 5 μM *syn*-(Me,Me)bimane in THF, in the presence of increasing concentrations of $NaBPh_4$ (λ_{ex} = 370 nm). The plots correspond to [$NaBPh_4$] = 0, 5.0×10^{-3}, 5.0×10^{-2}, 0.25, 0.50, 1.0, 2.5, 5.0, 7.5, 10.0 mM.

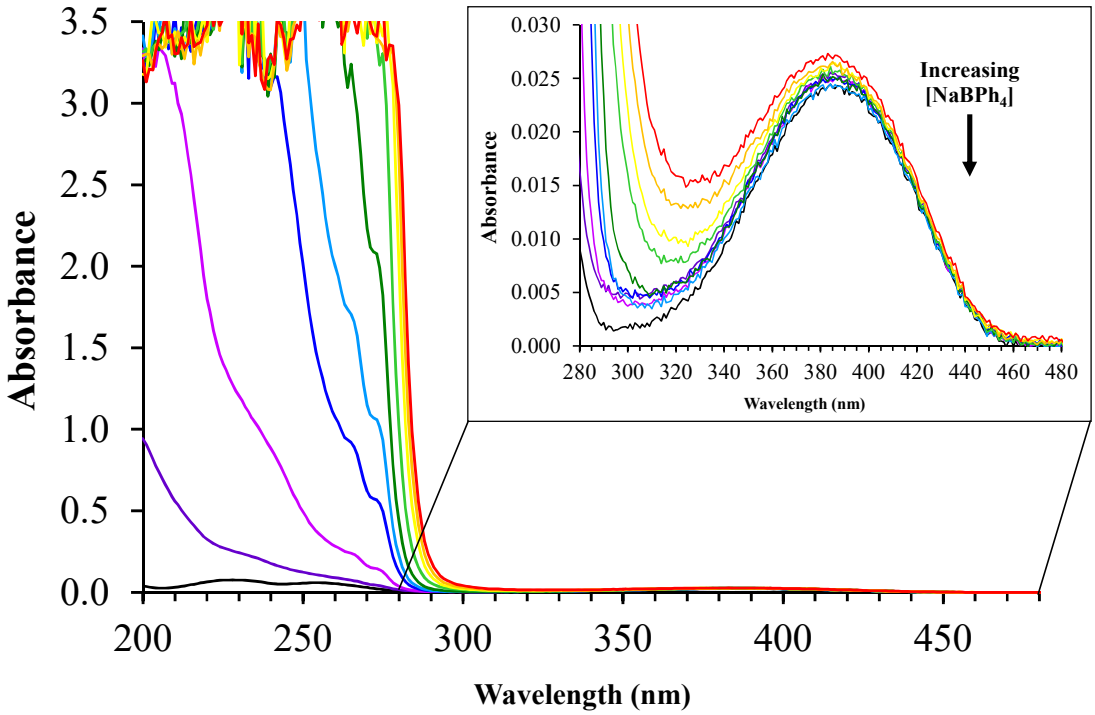

Figure S45. UV-Vis absorbance spectra of 5 μM mM *syn*-(Me,Me)bimane in H_2O, in the presence of increasing concentrations of $NaBPh_4$. The plots correspond to $[NaBPh_4] = 0, 5.0 \times 10^{-3}, 5.0 \times 10^{-2}, 0.25, 0.50, 1.0, 2.5, 5.0, 7.5, 10.0$ mM.

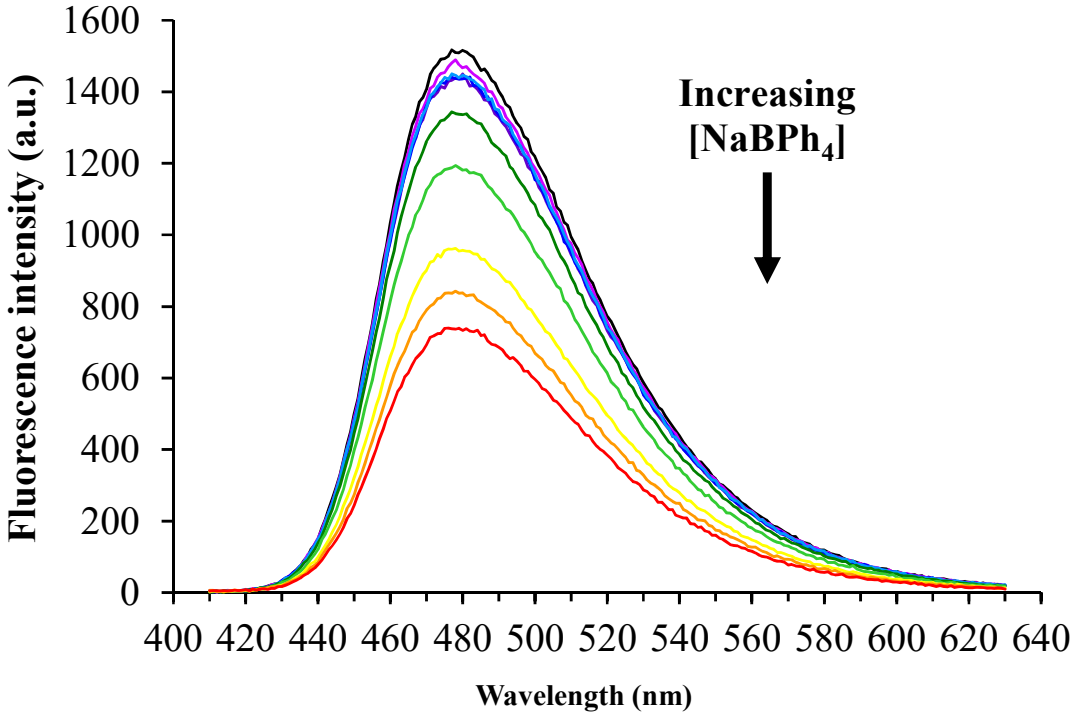

Figure S46. Fluorescence emission spectra of 5 μM *syn*-(Me,Me)bimane in H_2O, in the presence of increasing concentrations of $NaBPh_4$ (λ_{ex} = 385 nm). The plots correspond to $[NaBPh_4] = 0, 5.0 \times 10^{-3}, 5.0 \times 10^{-2}, 0.25, 0.50, 1.0, 2.5, 5.0, 7.5, 10.0$ mM.

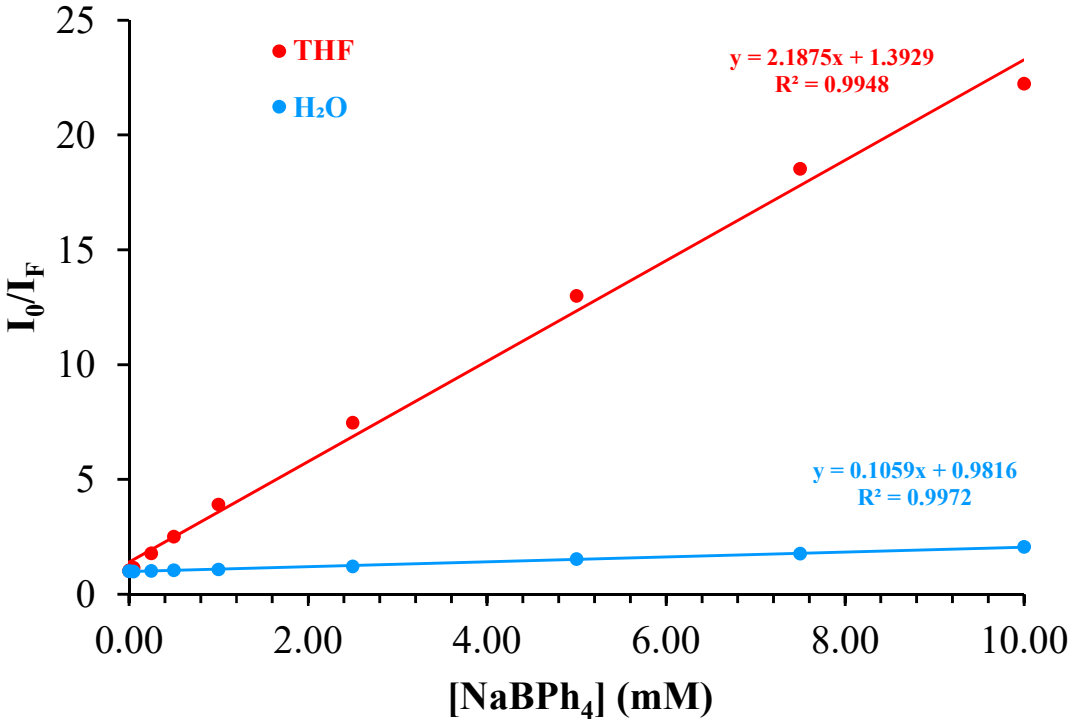

Figure S47. Stern-Volmer plots for the fluorescence quenching of 5 μM *syn*-(Me,Me)bimane by $NaBPh_4$ in THF and H_2O. The graphs were generated using the absorbance-corrected fluorescence data in Table S7. Each data point in the plots represents an average of at least 2 independent measurements.

Estimation of sodium-bimane binding constants and stoichiometry from fluorescence data. A simple model has been previously employed by numerous authors to assess the stoichiometry and binding constants involved in static quenching, wherein the fluorophore binds multiple units of a given quencher.[16] This model assumes an equilibrium reaction, $F + nQ \rightleftharpoons [FQ_n]$, where F is the fluorophore, Q is the quencher, and $[FQ_n]$ is a nonfluorescent complex. The fluorescence intensity is then related to the quencher concentration by the following equation:

$$\log\left(\frac{I_0 - I_F}{I_F}\right) = \log(K_A) + n\log[Q]$$

where I_0 and I_F are the fluorescence intensities in the absence and presence of the quencher, respectively; K_A is the equilibrium (binding) constant; and [Q] is the quencher concentration. By plotting $\log[(I_0-I_F)/I_F]$ as a function of log[Q], and provided that a good linear fit is obtained, it is possible to extract both K_A and n. We have adopted this approach to analyze the sodium-bimane system. Figure S48 shows the corresponding plots for THF and aqueous solutions containing *syn*-

[16] For examples, see: (a) J. Min, X. Meng-Xia, Z. Dong, L. Yuan, L. Xiao-Yu and C. Xing, *J. Mol. Struct.*, 2004, **692**, 71-80. (b) E. Froehlich, J. S. Mandeville, C. J. Jennings, R. Sedaghat-Herati and H. A. Tajmir-Riahi, *J. Phys. Chem. B*, 2009, **113**, 6986-6993.

(Me,Me)bimane and $NaBPh_4$, generated from the absorbance-corrected fluorescence data given in Table S5, which represent averaged values from at least 3 independent data sets. The plots exhibit good linearity.

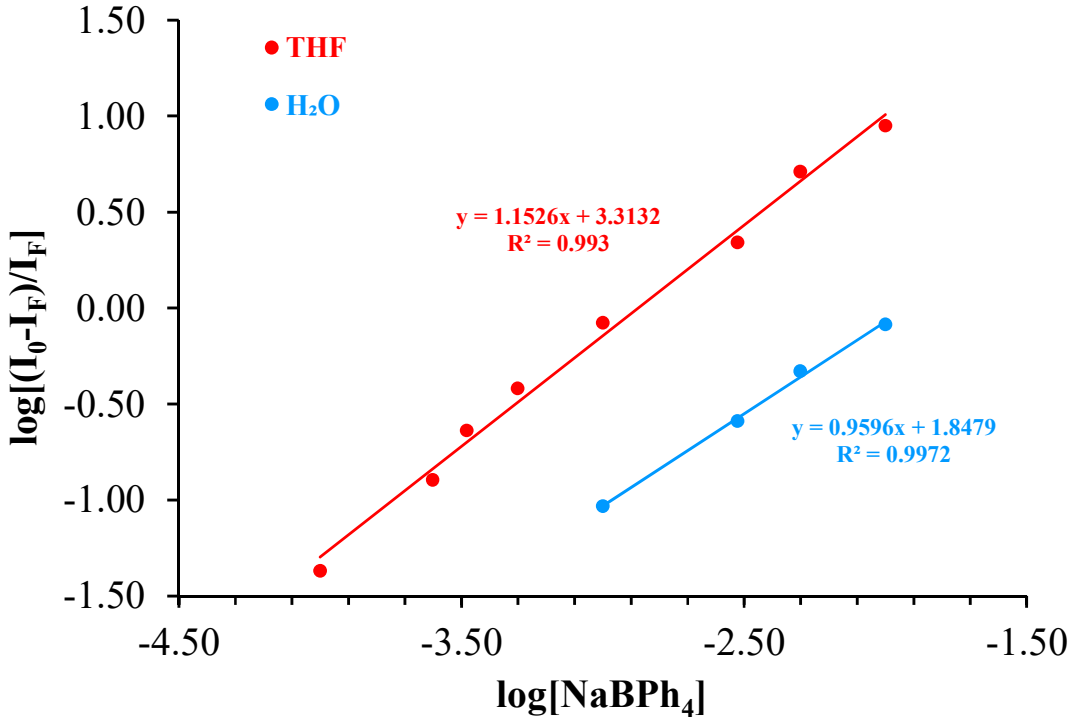

Figure S48. Plots of $\log[(I_0 - I_F)/I_F]$ as a function of $\log[NaBPh_4]$ for the fluorescence quenching of 1 mM *syn*-(Me,Me)bimane by $NaBPh_4$ in THF and H_2O. Each data point represents an average of at least 3 independent measurements.

Similar plots were drawn for each individual data set, giving the following results:

Solvent	Data set	*n*	log(K_A)	R^2
THF	1	1.18(8)	3.3(2)	0.9738
	2	1.02(3)	2.9(1)	0.9940
	3	1.3(1)	3.8(3)	0.9692
	4	1.21(3)	3.5(1)	0.9958
	Average:	*1.2(1)*	*3.4(4)*	-
H_2O	1	1.1(3)	2.3(7)	0.9057
	2	1.1(1)	2.1(3)	0.9825
	3	1.35(8)	2.7(2)	0.9926
	Average:	*1.2(1)*	*2.4(3)*	-

The results tabulated above indicate a roughly 1:1 molar ratio between *syn*-(Me,Me)bimane and $NaBPh_4$ in both THF and H_2O. They also show an apparent binding constant (K_A) of about 2500 in THF, and 250 in H_2O. It should be borne in mind that these constants include solvation contributions.

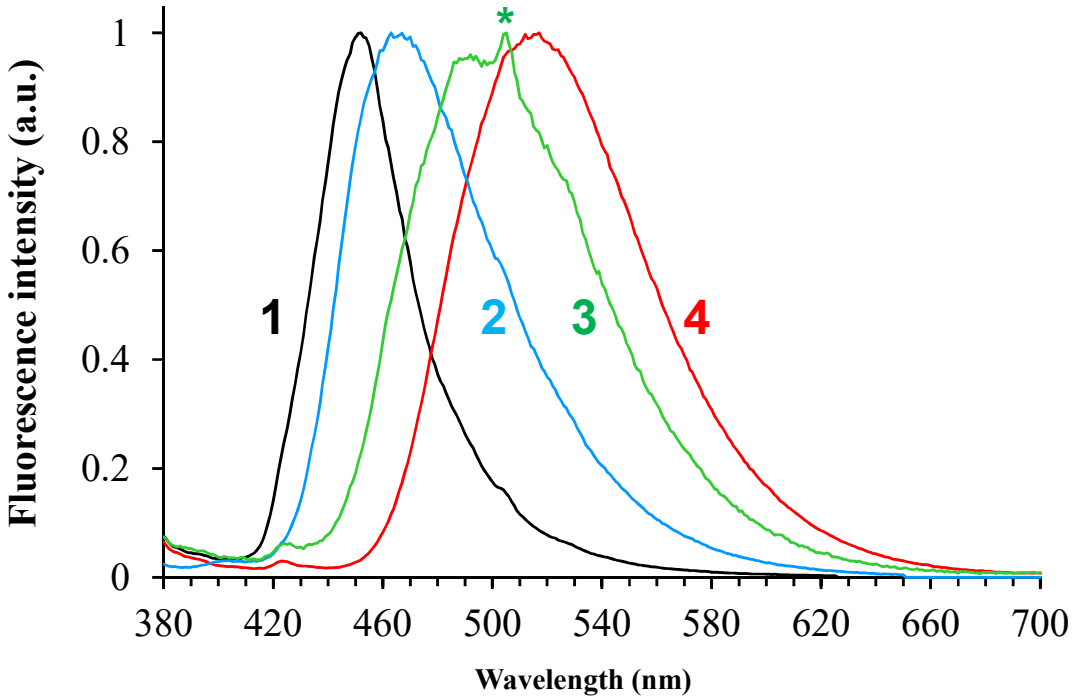

Figure S49. Solid-state fluorescence emission spectra of *syn*-(Me,Me)bimane (**1**) and complexes **2**-**4** (λ_{ex} = 370 nm). All compounds were suspended in mineral oil. The sharp peak marked with an asterisk (*) is an instrumentation artifact.

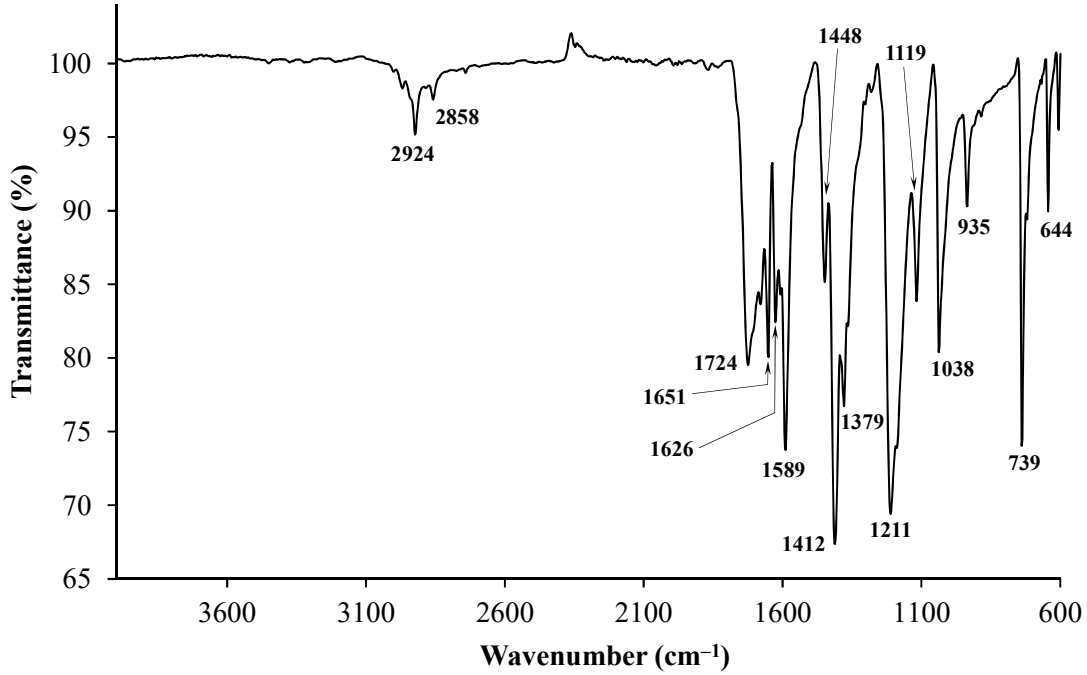

Figure S50. ATR infrared spectrum of solid *syn*-(Me,Me)bimane.

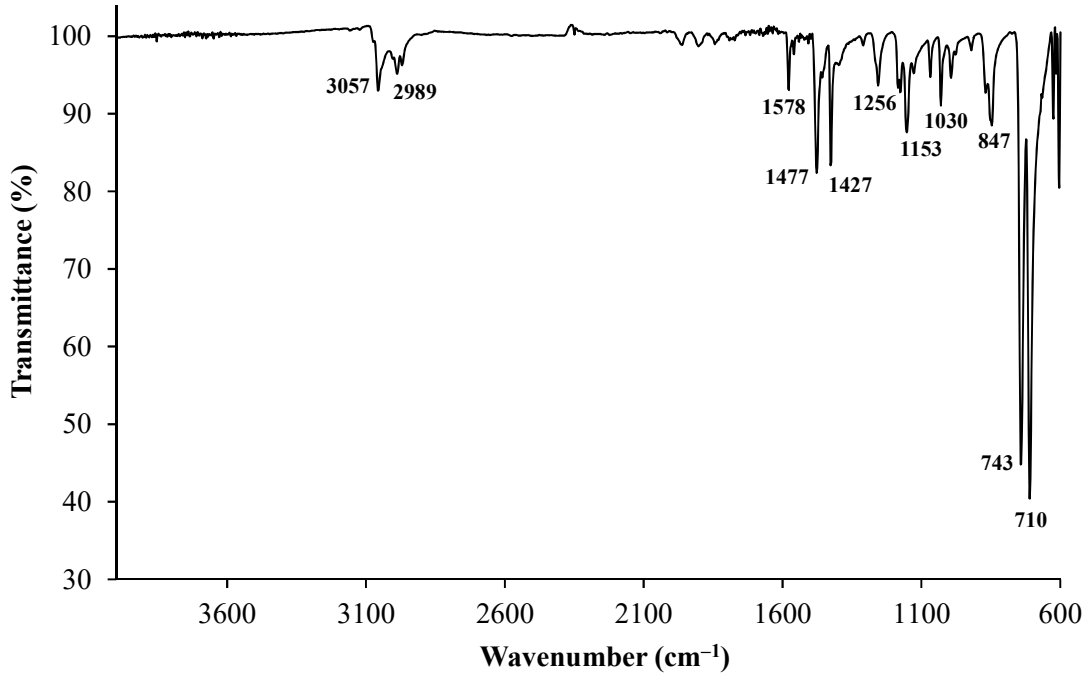

Figure S51. ATR infrared spectrum of solid $NaBPh_4$.

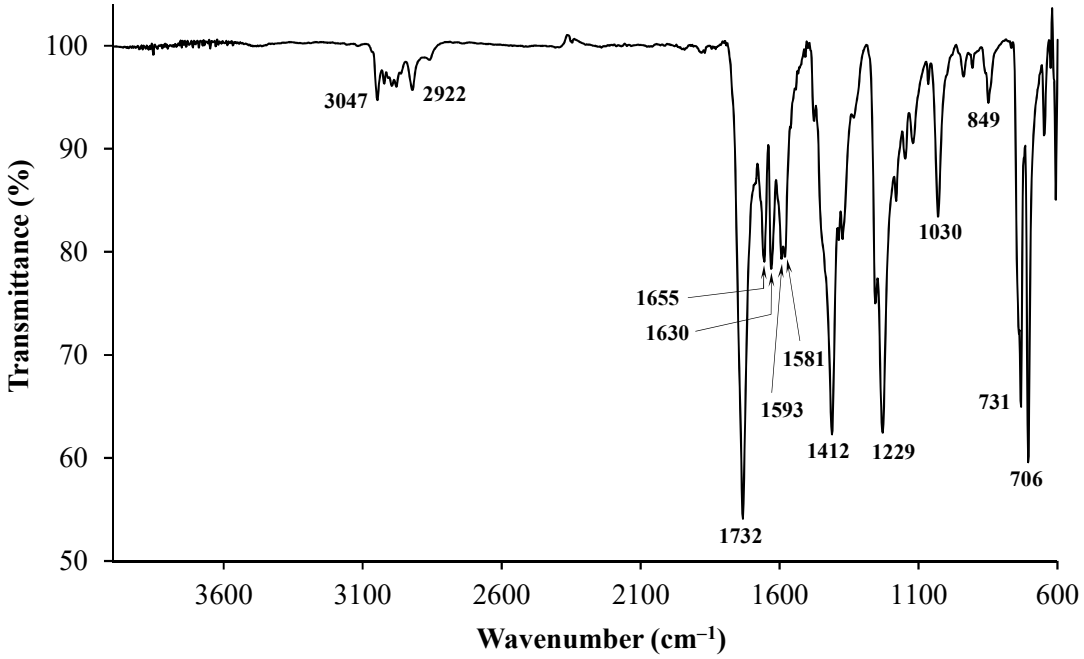

Figure S52. ATR infrared spectrum of crystalline complex **2**.

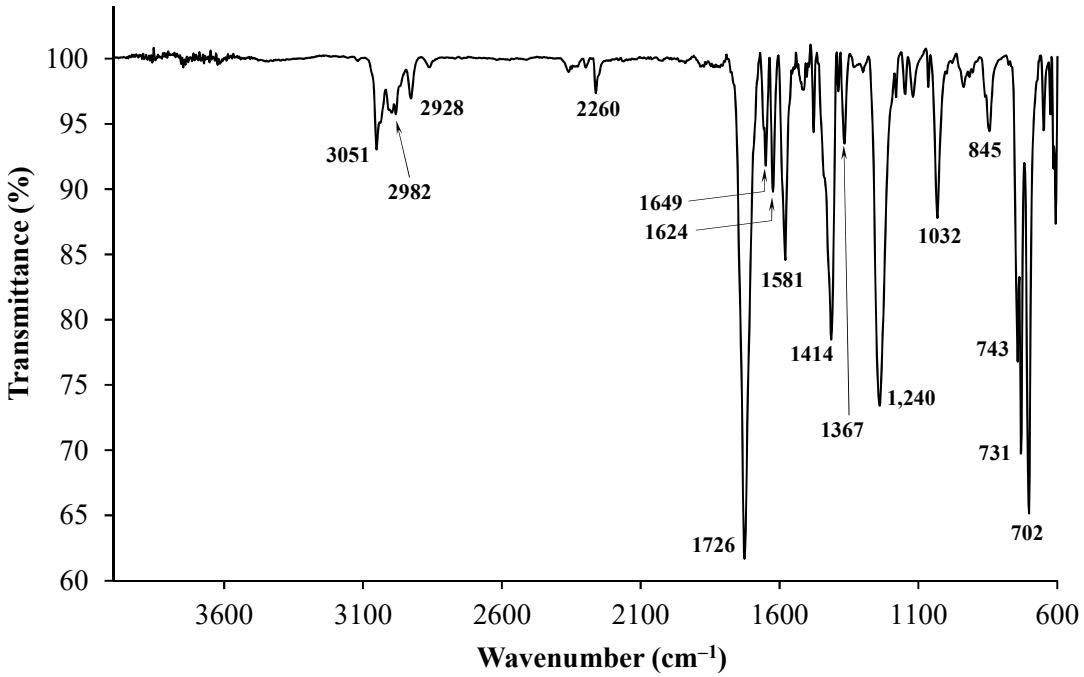

Figure S53. ATR infrared spectrum of crystalline complex **3**.

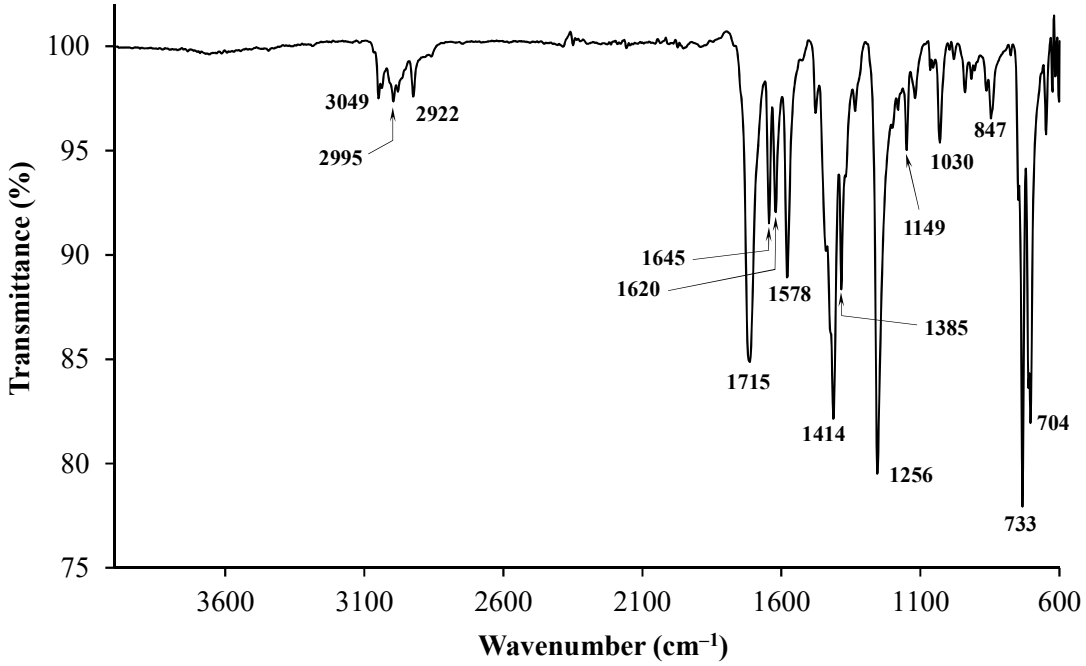

Figure S54. ATR infrared spectrum of crystalline complex **4**.